AD-A076 615 BOLT BERANEK AND NEWMAN INC ARLINGTON VA F/6 17/1
AN ALGORITHM FOR BEAM NOISE PREDICTION,(U)
MAY 79 M MOLL , R M ZESKIND , W L SCOTT N00173-77-C-0296
UNCLASSIFIED BBN-3653 NL

1 OF 2
AD A
076615

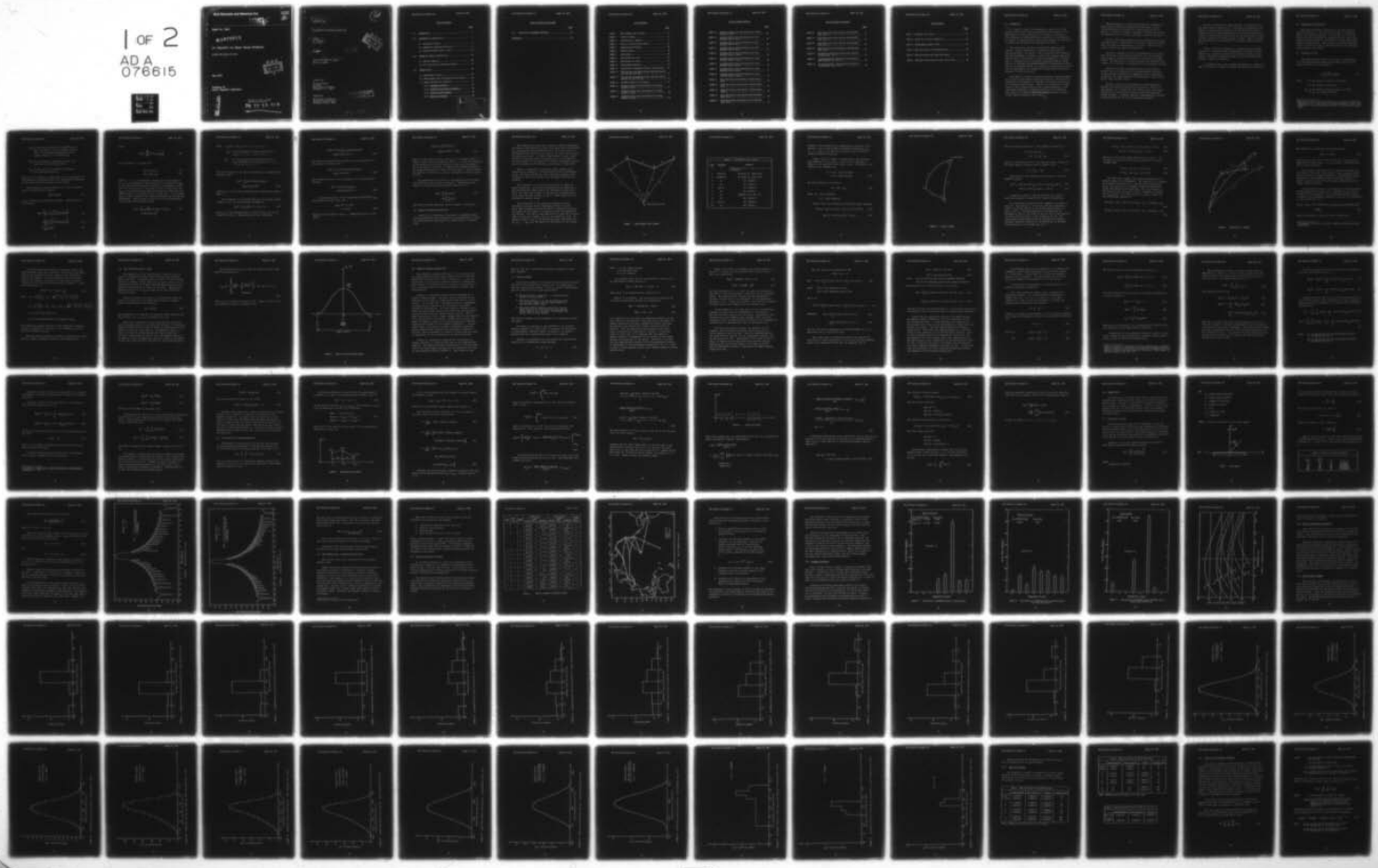

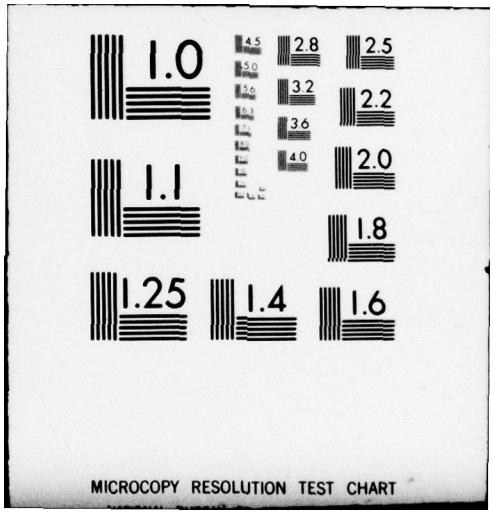
1.0
1.1
1.25
1.4
1.6
1.8
2.0
2.2
2.5
2.8
3.2
3.6
4.0
4.5
5.0
5.6
MICROCOPY RESOLUTION TEST CHART

Bolt Beranek and Newman Inc.

LEVEL II

Report No. 3653

An Algorithm for Beam Noise Prediction

M. Moll, R.M. Zeskind, W.L. Scott

May 1979

Prepared for:
Naval Research Laboratory

Approved for public release;
distribution unlimited

(12)

(14) BBN-
Report No. 3653

(6) AN ALGORITHM FOR BEAM NOISE PREDICTION,

(10) M./Moll
R. M./Zeskind
W. L./Scott

(11) May [redacted]79

(12) 102

(15) Contract No. N00173-77-C-0296
BBN Job No. 10601

Prepared for:

Dr. Orest Diachok
Code 8160
Naval Research Laboratory
Washington, D. C. 20375

Prepared by:

Bolt Beranek and Newman Inc.
1701 North Fort Myer Drive
Arlington, Virginia 22209

406 454

Table of Contents

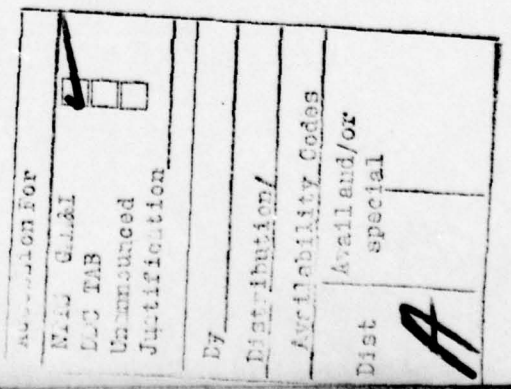

Table of Contents (concluded)

List of Figures

List of Figures (cont'd)

List of Figures (concluded)

List of Tables

1.0 INTRODUCTION

In a band of rather low frequencies, almost all of the ambient noise in the ocean is generated by ship traffic. The performance of sonars operating in this band is limited by this component of background noise; therefore, it is necessary to measure or predict certain statistical measures of beam noise to support system design and deployment decisions.

The probability measures of beam noise depend on many factors: array configuration, orientation, and location (including depth), and season. Thus it would be both expensive and time-consuming to attempt to obtain the required beam noise measures for a large number of sites experimentally. Furthermore, if shipping routes and traffic densities were to change because of strategic or economic causes, the measurements would have to be repeated. There is, therefore, considerable incentive for the development of a capability of predicting statistical measures of array beam noise.

The aspects of beam noise that should be considered depend on the type of performance predictions desired. For detection predictions, the quantity of interest is the total noise power in selected frequency bands. However, for prediction of false alarm or false classification rates, characterization of the narrowband components of shipping noise must be considered. Both aspects are addressed ~~in this report;~~ however, the bulk of the report pertains to the former.

The development of a beam noise prediction capability is partly based on prior work reported in Reference 1, which concerned prediction of noise at a receiving point due to ships in a sector of azimuth. Reference 2 introduced concepts and approaches that are more completely covered in Reference 1.

Certain input data required for the predictions are given in other reports. Characteristics of noise radiated by surface ships are given in References 3, 4, 6 and 7. Data on ocean route envelopes are given in Reference 5.

Sections 2 through 4 concern the prediction of the probability density of the random variable Y, the total averaged noise power in a specified passband at the output of a beamformer. The approach is to first calculate the characteristic function of Y, and then to transform it to the density function.

Section 2 presents an expression for Y, and derives a formula for the calculation of the characteristic function. It also defines a geometry for segmented routes, and derives a function that characterizes the distribution of ship coordinates normal to those routes.

Section 3 concerns the calculation of the probability density of Y from its characteristic function. Since Y is non-negative, it is shown that its density can be calculated from one of two alternative formulas, each involving only a single integral. A special numerical transformation technique is then derived for one of the alternative formulas.

Section 4 addresses the input data for the calculation of the characteristic function of Y, including a transmission loss function, a beam pattern function, and the geometry linking a specific sensor to the shipping routes in the surrounding ocean. A means is also devised and utilized for obtaining source characteristic functions for various types of ships. These functions are required for the calculation of the characteristic function of Y.

Section 5 derives a formula for calculating the expected value of N, a random variable representing the number of lines observed at a beamformer output whose center frequencies fall within a specified frequency interval, and whose average power exceeds a specified threshold.

A companion report, Bolt Beranek and Newman Inc. Report No. 3654, is entitled "A Computer Program for Beam Noise Prediction."

2.0 CHARACTERISTIC FUNCTION FOR Y

This section derives a formula for the characteristic function $\Phi_Y(\omega)$ for Y, the total noise power in a specified band at the beamformer output. It also deals with related matters such as a geometry for segmented routes, and a function that characterizes the distribution of ship coordinates normal to those routes. First however, the random variable Y will be stated in terms of the contributions of individual ships exposed to the sensor.

2.1 Derivation of $\Phi_Y(\omega)$

The averaged noise power at the output of a beamformer in a specified passband resulting from ship traffic in an acoustic basin* may be expressed as

$$Y = \sum_{i=1}^{m} \sum_{j=1}^{n} \sum_{k=1}^{A_{ij}} S_{ijk} Z_{ijk} B_{ijk} \qquad (1)$$

where m is the number of routes in the basin,

n is the number of ship types,

A_{ij} is the number of ships of type j on route i; A_{ij} is a random variable,

*The acoustic basin in which the array is located is defined by bathymetry (e.g., land masses and high underwater ridges.) The intensity of sound from sources outside of the basin is negligible.

S_{ijk} is the source intensity of the $k^{\underline{th}}$ ship of type j on route i; it is a random variable that is statistically independent of the source intensity of any other ship,

Z_{ijk} is the intensity transmission ratio from ship ijk to the receiving point,

B_{ijk} is the gain for a plane-wave arriving at the array from ship ijk.

Section 1.2 of Reference 1 shows that (1) is a consequence of the principle of superposition of the instantaneous pressures of the sound waves from multiple point sources.

The probability density function for Y can be obtained from its characteristic function

$$\Phi_Y(\omega) = E[\exp j\omega Y] \tag{2}$$

where E denotes the expectation operator. Substituting (1) in (2) gives

$$\Phi_Y(\omega) = E\left[\exp j\omega \sum_{i=1}^{m} \sum_{j=1}^{n} \sum_{k=1}^{A_{ij}} S_{ijk} Z_{ijk} B_{ijk}\right] \tag{3}$$

$$= E\left[\prod_{i=1}^{m} \prod_{j=1}^{n} \prod_{k=1}^{A_{ij}} \exp j\omega S_{ijk} Z_{ijk} B_{ijk}\right] \tag{4}$$

$$= \prod_{i=1}^{m} \prod_{j=1}^{n} \Phi_{ij}(\omega) \tag{5}$$

where

$$\Phi_{ij}(\omega) = E\left[\prod_{k=1}^{A_{ij}} \exp j\omega S_{ijk} Z_{ijk} B_{ijk}\right] \tag{6}$$

In the sequel it is assumed that

$$Z_{ijk} = z(G_{ijk}, Q_{ijk}) \tag{7}$$

$$B_{ijk} = b(G_{ijk}, Q_{ijk}) \tag{8}$$

where $z(\ ,\ )$ is a deterministic transmission ratio function; $b(\ ,\ )$ is a deterministic gain function for a plane-wave; G_{IJK} is the earth-centered angle measuring the longitudinal coordinate (in the direction of the nominal route) of ship ijk; and Q_{ijk} is the earth-centered angle measuring the transverse coordinate (normal to the nomial route) of ship ijk. It is assumed that all ship coordinates are random variables that are mutually independent. Substituting (7) and (8) in (6) and performing the expected-value operation gives

$$\Phi_{ij}(\omega) = \sum_{a=0}^{\infty} p_{ij}(a)\left[\int dg f_{G_i}(g) \int dq f_{Q_i}(q;g) \int ds f_{Sj}(s) \times \exp j\omega s z(g,q) b(g,q)\right]^a \tag{9}$$

where $p_{ij}(a) = P(A_{ij} = a)$; $a = 0, 1, 2, 3, \ldots$

$f_{G_i}(\ )$ is the probability density function for G_{ijk}; $j = 1, 2, \ldots,$ $k = 1, 2, 3, \ldots$

$f_{Q_i}(\ ,\ )$ is the probability density function for Q_{ijk} depending on the variable g; $j = 1, 2, \ldots, n$; $k = 1, 2, 3, \ldots$

The inner integral of (9) can be expressed as a characteristic function; thus

$$\Phi_{ij}(\omega) = \sum_{a=0}^{\infty} p_{ij}(a) \{ \int dg F_{Gi}(g) \int dq f_{Qi}(q;g) \times \Phi_{Sj}[\omega z(g,q) b(g,q)] \}^a \qquad (10)$$

where $\Phi_{Sj}(\ )$ is the source characteristic function for ships of type j.

In the sequel, it is assumed that A_{ij} is a Poisson random variable; thus, its probabilities are given by

$$p_{ij}(a) = \exp(-a_{ij}) a_{ij}^a \div a!, \quad a = 0, 1, 2, 3, \ldots \qquad (11)$$

where a_{ij} is the average number of ships of type j in an increment of route i. Substituting (11) into (10) gives

$$\Phi_{ij}(\omega) = \exp(-a_{ij}) \sum_{a=0}^{\infty} \{a_{ij} \int dg f_{Gi}(g) \int dq f_{Qi}(q;g) \times \Phi_{Sj}[\omega z(g,q) b(g,q)]\}^a \div a! \quad (12)$$

The sum is the power series expansion for the exponential of the quantity in braces; thus

$$\Phi_{ij}(\omega) = \exp(-a_{ij}) \exp\{a_{ij} \int dg f_{Gi}(g) \int dq f_{Qi}(q;g) \times \Phi_{Sj}[\omega z(g,q) b(g,q)]\} \quad (13)$$

The cumulant function is the logarithm of the characteristic function

$$\Psi_{ij}(\omega) = a_{ij} \{\int dg f_{Gi}(g) \int dg f_{Qi}(q,g) \times \Phi_{Sj}[\omega z(g,q) b(g,q)] - 1\} \quad (14)$$

If the distributions of the longitudinal coordinates G_{ijk} are uniform over the route, then

$$f_{Gi}(g) = \ell^{-1}, \ 0 \leq g \leq \ell_i$$
$$= 0, \text{ elsewhere} \quad (15)$$

where ℓ_i is the length of route i. Substituting (15) in (14) yields

$$\psi_{ij}(\omega) = \rho k_{ij} \int_0^{\ell_i} dg \int dq f_{Qi}(q,g)$$

$$\times \Phi_{Sj}[\omega z(g,q) b(g,q)] - \rho \ell_i k_{ij} \qquad (16)$$

where ρ is the earth's radius, and k_{ij} is the average number of ships of type j per unit length of route i. In (16) the variables of integration are the route variables g and q; an alternative set of variables is the pair of observation variables related to the range and bearing of a point from the sensor. These variables are defined in Section 2.2, and the alternative to (16) is given by (33).

The characteristic function is the exponential of the cumulant function; thus, $\Phi_{ij}(\omega) = \exp \psi_{ij}(\omega)$. Substituting this result in (5) gives the characteristic function of Y

$$\Phi_Y(\omega) = \prod_{i=1}^{m} \prod_{j=1}^{n} \exp \psi_{ij}(\omega) \qquad (17)$$

$$= \exp \sum_{i=1}^{m} \sum_{j=1}^{n} \psi_{ij}(\omega)$$

The second of these equivalent forms is easier to calculate.

2.2 Geometry for Beam Noise Prediction

Section 2.2 of Reference 1 discusses a coordinate system that is applicable to the prediction of characteristics of noise at a point received from ships in a narrow sector of observation.

The prediction of beam noise, however, requires accounting for sidelobe contributions as well as the main lobe contribution. As a consequence, the observation sector for a given route is determined by the extent of the route in the basin that includes the observation point. A further complication is that within a basin a route may consist of several great circle segments. For these reasons it is important to devise a coordinate system that is suitable for the efficient calculation of beam noise.

Figure 1 illustrates a route with three segments with end-points R_1 through R_4. The observation point is designated by R_0. This case defines the three spherical triangles shown in Figure 1, which also defines arcs and angles that will be required.

The calculation of $\Phi_Y(\omega)$ will be executed in spherical polar coordinates. One of the coordinates is the range arc r, the earth-centered angle between the observation point and a ship. For each route segment i, an angle D_i is defined which is the angle between the arcs s_i and r. These angles will be discussed in greater detail.

The calculation of the parameters required for the calculation of $\Phi_Y(\omega)$ can be organized by means of a data array whose headings are shown in Table 1, along with explanatory notes and the numbers of figures in which the parameters are defined. The order of data generation is from top to bottom. Item 0 is the point number, that is, the subscript of R_i. As shown in Figure 1, R_0 is the observation point, and points R_1, R_2, R_3, ..., R_{n+1} are the numbers of end-points of the n route

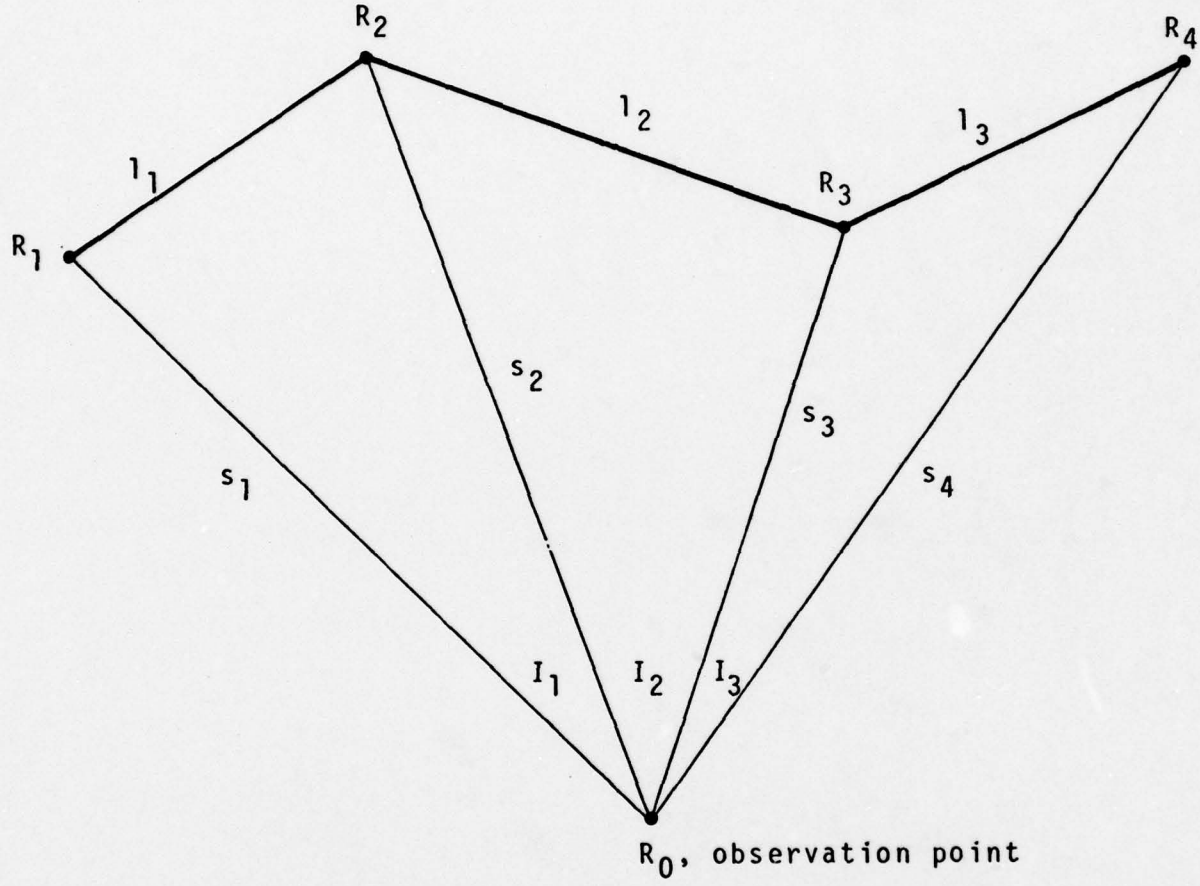

FIGURE 1 Route Segments and Triangles

Table 1: Parameters for a Route

Item	Heading	Comments
0	i	subscripts of R_i, i = 0, 1, 2, 3, ..., n, Figure 1
1	latitude	of point R_i, input data
2	longitude	of point R_i, input data
3	c_i	(1), Figure 2
4	N_i	(2), Figure 2
5	cos s_i	(3), Figure 2
6	C_i	(4), Figure 2
7	Z_i	azimuth of R_i, Eq. (5)
8	I_i	(6), Figure 1
9	sin l_i	(7), Figure 1
10	F_i	(8), Figure 1

segments. The convention for numbering the end-points is as follows: from a point within the spherical polygon R_0, R_1, R_2, ..., R_{n+1}, R_1 is the route end-point that is the more counter-clockwise around R_0.

Items 1 and 2 of Table 1 are input data, the latitudes and longitudes of the points. Items 3 and 4, defined in Figure 2, are calculated from Items 1 and 2. The sides of the (north) polar triangles are

$$\begin{aligned} c_i &= \pi/2 - \text{north latitude} \\ &= \pi/2 + \text{south latitude} \end{aligned} \tag{18}$$

The polar angles N_i are given by

$$N_i = |W_i - W_0| \tag{19}$$

where W_i = west longitude

= 2π - east longitude

Items 5 and 6 are obtained by solving the polar triangles

$$\cos s_i = \cos c_i \cos c_0 + \sin c_i \sin c_0 \cos N_i \tag{20}$$

$$\sin C_i = \sin c_i \sin N_i \div \sin s_i \tag{21}$$

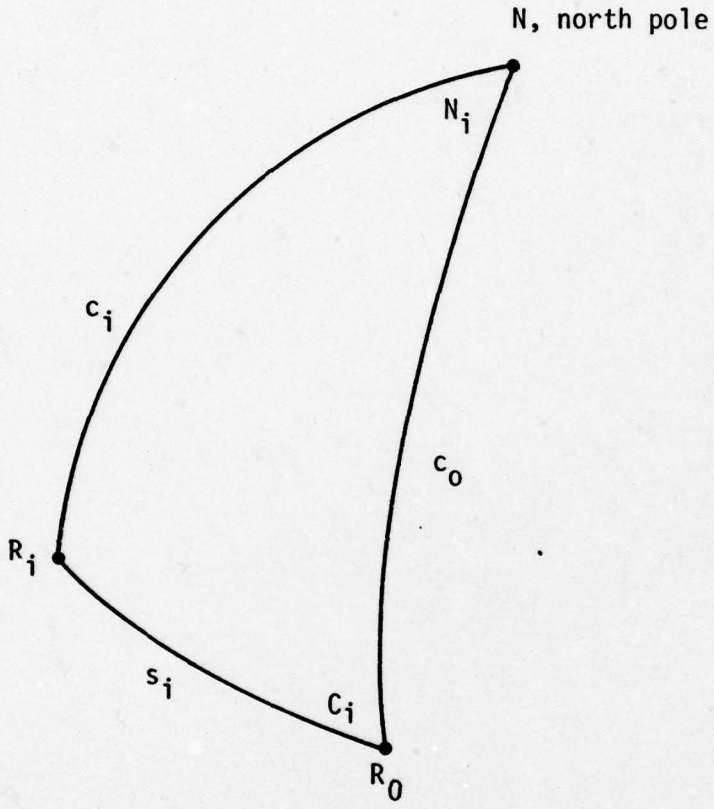

FIGURE 2 A Polar Triangle

Item 7 is derived from Item 6. The azimuth of point R_i is

$$z_i = C_i, \; W_i \leq W_0$$
$$= 2\pi - C_i, \; W_i > W_0 \qquad (22)$$

where W_i is given below (19). The internal angles (Item 8) of the route segment triangles shown in Figure 1 are

$$I_i = |z_{i+1} - z_i| \qquad (23)$$

Items 9 and 10 are obtained from solutions of the route segment triangles

$$\cos l_i = \cos s_i \cos s_{i+1} + \sin s_i \sin s_{i+1} \cos I_i \qquad (24)$$

$$\sin F_i = \sin s_{i+1} \sin I_i \div \sin l_i \qquad (25)$$

It might be useful to add the item $\sin s_i$ to Table 1 since this quantity is required for several calculations.

The observation variables in route segment i are shown in Figure 3. The variable r_i is the arc from the observation point to the ship, and D_i is the surface angle between the arcs s_i and r_i. The ship position is also given by the variables g_i and q_i; the former is the arc R_iT in the direction of travel, and the latter is the transverse arc TS. The relationship between these pairs of variables is required. Auxiliary variables involved in the derivation are obtained from solutions of the triangle R_0, R_1, S:

$$\cos d_i = \cos s_i \cos r_i + \sin s_i \sin r_i \cos D_i \quad (26)$$

$$\sin R_i = \sin r_i \sin D_i \div \sin d_i \quad (27)$$

where R_i is the surface angle between arcs s_i and d_i. The variables g_i and q_i are found from solutions of the right triangle $R_i ST$:

$$\tan g_i = \cos (R_i - F_i) \tan d_i \quad (28)$$

$$\sin q_i = \sin (R_i - F_i) \sin d_i \quad (29)$$

For each route segment, the following numerical integration regime can be considered. The variable D_i is advanced in increments from zero to I_i, and for each selected value of D_i, the variable r_i is stepped through the appropriate range, determined per the following. For a ship that is on the nominal track, the points S and T in Figure 3 coincide, as do d_i and g_i. The first value of r_i used is found from the simultaneous solution of

$$\tan \tfrac{1}{2}(r_i - g_i) = \tan \tfrac{1}{2} s_i \sin \tfrac{1}{2}(F_i - D_i) \div \sin \tfrac{1}{2}(F_i + D_i) \quad (30)$$

$$\tan \tfrac{1}{2}(r_i + g_i) = \tan \tfrac{1}{2} s_i \cos \tfrac{1}{2}(F_i - D_i) \div \cos \tfrac{1}{2}(F_i + D_i) \quad (31)$$

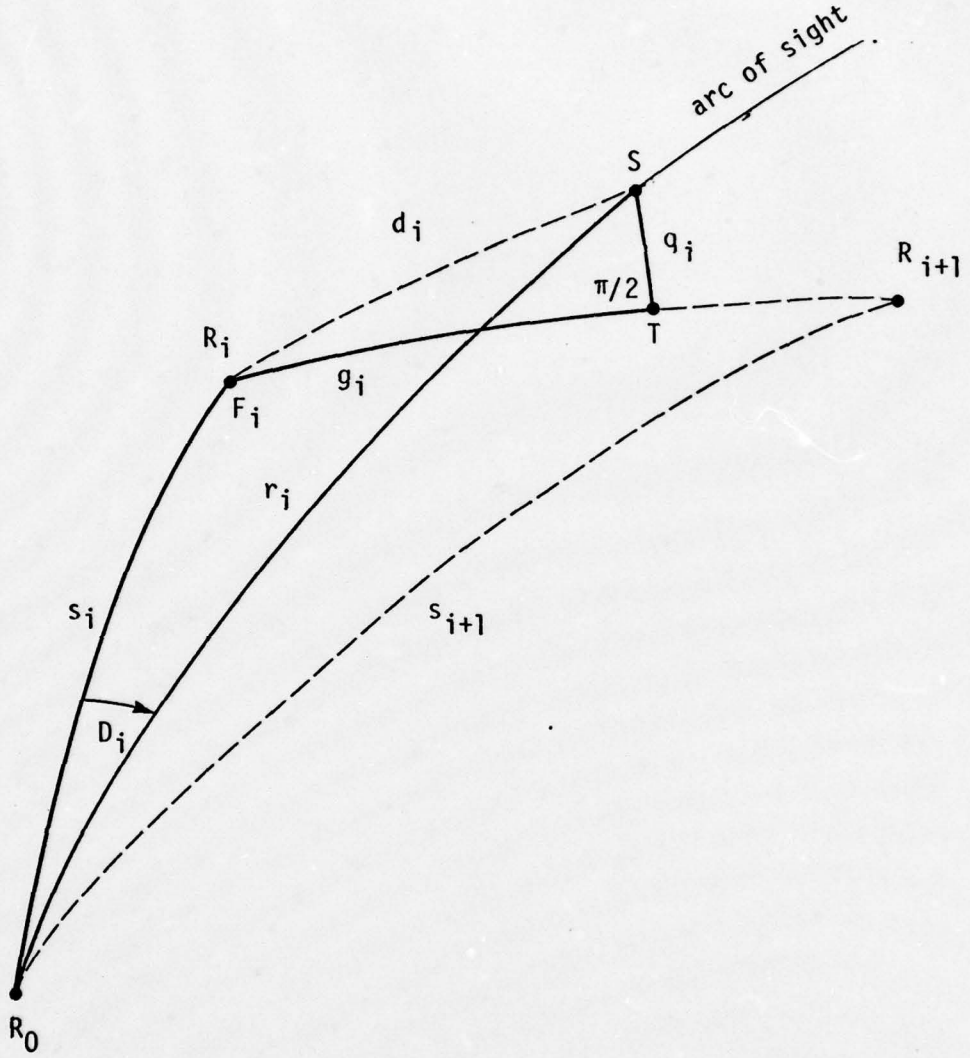

FIGURE 3 Coordinates in a Segment

The variable r_i is increased by increments until

$$|g_i| \geq \tfrac{1}{2} w_i(g_i) \tag{32}$$

where $w_i(g)$ is the width of the route at g_i. Then starting again at the initial value of r_i, the value is decreased until (32) is again satisfied.

The procedure described does not completely characterize the routes at the turns, and partially self-cancelling errors will occur near the segment end-points. This problem could be remedied in a straightforward fashion with the expense of greater complexity, which does not appear warranted with the current state of the art.

In the previous section, a formula used in the calculation of the characteristic function of Y employed the ship route variables in the integrals. This formula may now be restated in terms of the observation variables r and D.* The alternative to (16) of Section 2.1 is.

$$\psi_{ij}(\omega) = \rho k_{ij} \int dr \int dD|J(r,D)| \, f_{q_i}(g,q) \, \Phi_{Sj} \, [\omega z_t(r,D) b_t(r,D)] - \rho \ell_i k_{ij} \tag{33}$$

where the Jacobian is given by (2-23) of Reference 1.

*To simplify the result, the route segment subscript has been suppressed.

A recently distributed report [5] presents certain data characterizing ocean route envelopes: the latitude and longitude of the end-points of route segments; the (transverse) width of the segments at their end-points; and the maximum width of the segment. The width of a route may be given as a function of the distance travelled along a segment. A quadratic formulation is

$$w_i(g_i) = w_i + b_i g_i + e_i g_i^2 \qquad (34)$$

where $$b_i = 2\,\ell_i^{-1}\left[m_i - w_i + \sqrt{(m_i - w_i)\,(m_i - w_{i+1})}\right]$$

$$e_i = \ell_i^{-2}\left[(m_i - w_i) + (m_i - w_{i+1}) + \sqrt{(m_i - w_i)\,(m_i - w_{i+1})}\right]$$

w_i is the route width at R_i

m_i is the maximum width of the segment R_iR_{i+1}

The probability density function of the transverse coordinates Q_i may be expressed as a function of the variable q_i and the (variable) parameter $w_i(g_i)$.

The next section derives a function to represent the distribution of ships' coordinates normal to the nominal route.

2.3 Ship Distribution Across a Route

The computation of the characteristic function $\Phi_Y(\omega)$ requires a probability density function for the ship position across the route. In Equation (33) of Section 2.2 this density function is denoted for the $i^{\underline{th}}$ route by $f_{Q_i}(q)$, where q is the earth-centered angle in radians representing across-route ship position measured from the center of the route. This section develops a function for $f_{Q_i}(q)$ based on the beta probability density function.

Define the width of the route, at a given point along the route, as W, where W is an earth-centered angle in radians. Define the half-width of the route as

$$q_o = (1/2)W \tag{35}$$

The probability of a ship that is using this route being outside the interval $-q_o \leq q \leq + q_o$ is assumed to be zero.

Since exact information of ship distributions across the world's shipping routes is not presently available, a probability density function must be chosen to model the uncertainty in ship position within the route width W. An appropriate choice is felt to be the beta probability density function with the parameter values both set equal to two. This density function is symmetric about its mean value, which if chosen as the center of the route, does not favor one side of a route over the other.

The density function to be used for across the route ship position uncertainty is

$$f_{Q_i}(q) = \begin{cases} \frac{1.875}{2q_o}\left(1-\left(q/q_o\right)^2\right)^2, & \text{for } -q_o \leq q \leq +q_0 \\ 0, & \text{otherwise} \end{cases} \tag{36}$$

Where q_o is as defined in Equation (35). Figure 4 shows a plot of the density function of Equation (36).

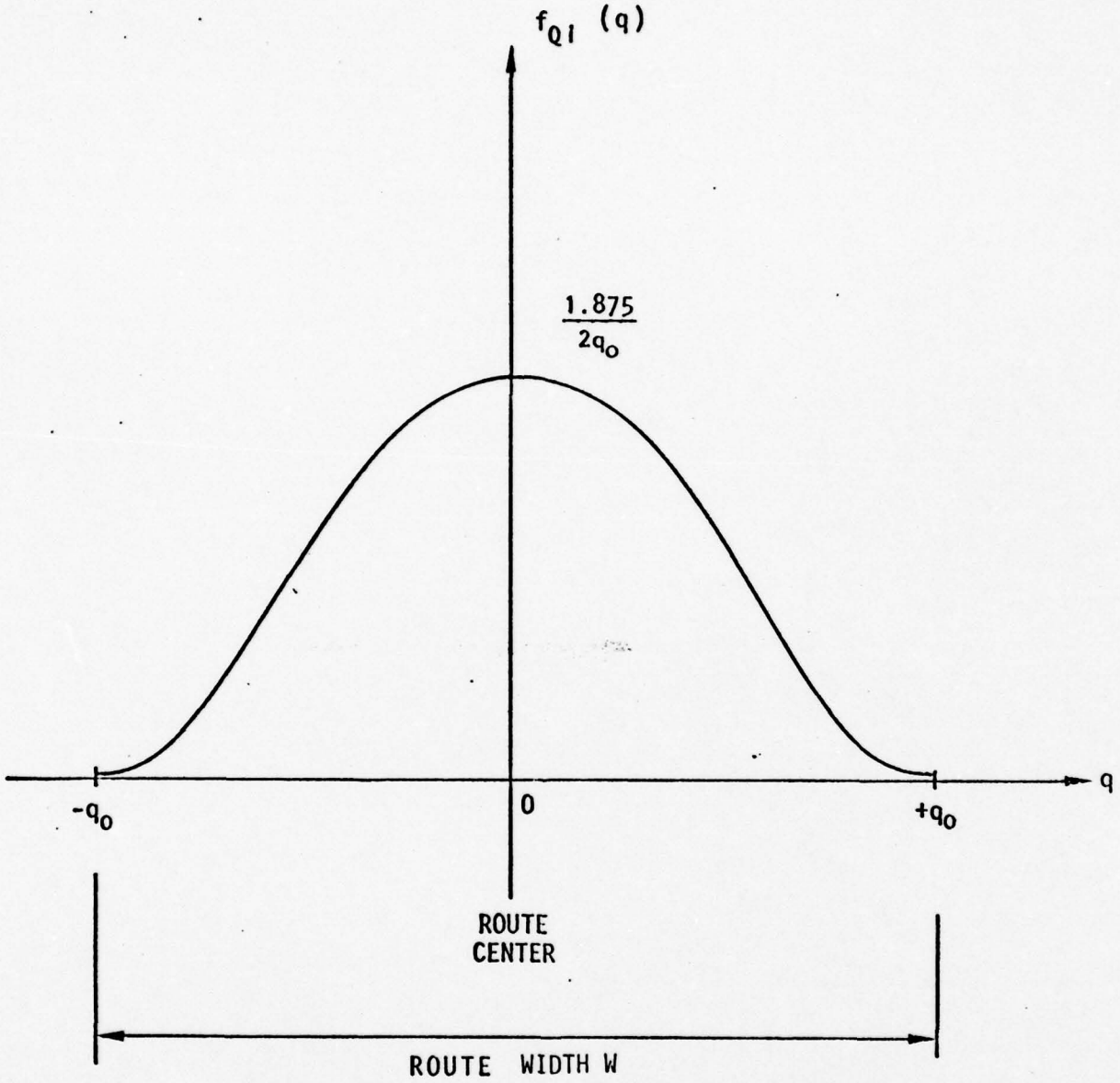

FIGURE 4 Density of Position Across Route

3.0 PROBABILITY DENSITY FUNCTION FOR Y

The probability density function of Y is calculated from its characteristic function $\Phi_Y(\omega)$, which in turn is obtained using (33) of Section 2.2 in (17) of Section 2.1. Since the calculation is to be done by numerical methods, consideration must be given to selecting a set of values of ω at which Φ_Y is to be calculated, and to an efficient method to achieve its transformation.

Section 3.1 considers several factors pertaining to a uniform sampling scheme. The first factor considered is the reduction of the number of sample values that have to be calculated. It is shown that a technique similar to basebanding in communications systems is not effective if the random variable is non-negative. For such variables, however, it is shown that alternative forms are available for calculating the density function from the characteristic function. Each of these forms involve only a single integral *vice* the two required for a variable not so restricted. Another way to reduce the number of samples required is to employ higher-order function interpolation schemes for the density calculation. A second-order scheme is selected to provide a reasonable compromise between sample number reduction and calculation complexity. The final factor considered is a means of stabilizing the range of integration in the calculation of the density function.

Section 3.2 develops an algorithm for calculating the density function of Y from the real part of the characteristic function. The method developed is attractive in that the selection of the inter-sample interval does not depend on the value of the probability density variable y. This would not have

been the case had a conventional numerical integration scheme been employed.

3.1 Function Sampling

The previous version of the ambient noise prediction program calculated the characteristic function of Y at frequencies ω_i that were exponentially spaced. There are several disadvantages that are inherent in this sampling procedure.

- No calculation is made for $\omega = 0$ (This would be useful as a check point.)
- The space between $\omega = 0$ and the smallest value of ω is much larger than the space between it and the next larger value.
- The space between adjacent values of ω at the upper range is so large that the approximation of the function as a straight line between the points lead to large errors.

This section concerns the investigation of an alternative sampling regime.

One factor to consider is the reduction of the required number of samples by a method that is analogous to the practice of heterodyning a bandpass signal to baseband. The general possibilities are illustrated by means of two examples.

Consider the possibility of calculating the characteristic function for a standardized random variable

$$S = (X - m) \div \sigma \qquad (37)$$

where x is any random variable
m is its mean value
σ^2 is its variance

It is easily shown that the characteristic function for the standardized random variable is

$$\Phi_S(\omega) = \exp(-j\omega m \div \sigma)\ \Phi_X(\omega \div \sigma) \tag{38}$$

where $\Phi_X(\omega)$ is the characteristic function for X.

Suppose X is Gaussian. The characteristic functions for it and the standardized variable are respectively

$$\Phi_X(\omega) = (\exp jm\omega)\exp - \tfrac{1}{2}(\sigma\omega)^2 \tag{39}$$

$$\Phi_S(\omega) = \exp - \tfrac{1}{2}\omega^2 \tag{40}$$

It is apparent from (39) that the modulation frequency of the first factor is proportional to the mean value; the number of samples required for accurate sampling is thereby increased. The spread of the second factor varies inversely with the variance. Thus the sampling problem induced by the first factor increases with a decrease in variance. If the mean value of X were zero, it is surmised that the number of samples required is independent of the variance if the sample spacing is proportional to the spread. From (40) it is seen that the characteristic function for the standardized variable is independent of the distribution parameters of X, i.e., m and σ; thus, a fixed sampling routine with a minimal number of points could be used.

Suppose next that X is uniformly distributed between a - b and a + b. In this case the characteristic functions for X and S are respectively

$$\Phi_X(\omega) = (\exp ja\omega)\ (\sin b\omega \div b\omega) \tag{41}$$

$$\Phi_S(\omega) = \sin \sqrt{3}\omega \div \sqrt{3}\omega \tag{42}$$

For this distribution m = a, and it is seen that the modulating effect of the non-zero mean is identical to that discussed before. The characteristic function for the standardized variable is again seen to be independent of the distribution parameters of X. In this case, however, the function oscillates, and might require more samples than the Gaussian case.

In both examples it is noted that one of the distribution parameters affects only the displacement of the function, and that the other affects only its spread. Furthermore, both functions have even symmetry about the mean value, with the consequence that the characteristic function for the standardized variables has an imaginary part that is identically zero.

For the noise prediction model, the variable is non-negative, and in general the density function will not be evenly symmetric about the mean. Thus the imaginary part of the characteristic function for the standardized variable will not be identically zero. Furthermore, if the ratio of σ/m is high, the density will be high near small positive values; displacing the curve by the amount of the mean value will have the undesirable effect of displacing the highest density region from zero.

One fact that can be exploited is that

$$f(x) = 0, \quad x < 0$$

Now $$f(x) = \frac{1}{\pi} \int_0^\infty d\omega \; R(\omega) \cos \omega x + \frac{1}{\pi} \int_0^\infty I(\omega) \sin \omega x \qquad (43)$$

where $R(\omega)$ is the real part of $\Phi(\omega)$

$I(\omega)$ is the imaginary part of $\Phi(\omega)$

For $x > 0$

$$f(-x) = \frac{1}{\pi} \int_0^\infty d\omega \; R(\omega) \cos \omega x - \frac{1}{\pi} \int_0^\infty d\omega \; I(\omega) \sin \omega x = 0 \qquad (44)$$

Therefore $$f(x) = \frac{2}{\pi} \int_0^\infty d\omega \; R(\omega) \cos \omega x, \quad x \geq 0 \qquad (45)$$

$$= \frac{2}{\pi} \int_0^\infty d\omega \; I(\omega) \sin \omega x, \quad x \geq 0 \qquad (46)$$

That is, $f(x)$ can be expressed as a single integral for $x \geq 0$, and either (45) or (46) can be used.

This result does not drastically reduce the computation load since to obtain either $R(\omega)$ or $I(\omega)$, both real and imaginary parts of the cumulant function must be computed; that is

$$R(\omega) = \exp S(\omega) \cos J(\omega) \tag{47}$$

$$I(\omega) = \exp S(\omega) \sin J(\omega) \tag{48}$$

where $S(\omega)$ is the real part of the cumulant function

$J(\omega)$ is the imaginary part of the cumulant function

Substituting (47) in (45) and (48) in (46) yields

$$f(x) = \frac{2}{\pi} \int_0^\infty d\omega \exp S(\omega) \cos J(\omega) \cos \omega x, \; x \geq 0 \tag{49}$$

$$= \frac{2}{\pi} \int_0^\infty d\omega \exp S(\omega) \sin J(\omega) \sin \omega x, \; x \geq 0 \tag{50}$$

Although (49) and (50) are equivalent to (45) and (46) respectively, the method of their calculation could be significantly different.

Aside from the exponential spacing of the sample points, the approach taken in Reference 1 for the evaluation of (43) has considerable merit. In that approach, the components of the characteristic function are approximated by linear functions between data points. The resulting integrals are evaluated analytically. This allows the sampling regime to be dictated solely by the components of the characteristic function. This is very desirable because the trigonometric functions in the integrands of (43) vary rapidly with ω with large values of x. The same approach can be considered for the calculation of (49) or (50), a practice that would be desirable only if $S(\omega)$ and $J(\omega)$ have a smaller "bandwidth" than $R(\omega)$ or $I(\omega)$. If $S(\omega)$ and $J(\omega)$ are represented as linear functions between data points, the integrals can be evaluated analytically.

An alternative that can be considered is to represent the components as $n^{\underline{th}}$ order polynomials in the interval between n + 1 data points. With either (45) or (46) the integrals would be easy to evaluate. The same approach with (49) and (50) would probably be intractable if n is two or more.

At this point the development of (45) and (46) for n = 2 seems an attractive possibility.

All of the results of interest can be restated for a normalized variable. If it were possible to determine in advance that $f(x) = 0$, $x \leq q > 0$, and if q is not small compared to σ, then it would be worthwhile to compute the characteristic function for the variable

$$T = (X - q) \div \sigma \tag{51}$$

However, if q cannot be determined, or if it is small compared to σ, then the reasonable recourse is to calculate the functions for

$$U = X \div \sigma \tag{52}$$

which are

$$\Phi_U(\omega) = \Phi_X(\omega \div \sigma) \tag{53}$$

and

$$\psi_U(\omega) = \psi_X(\omega \div \sigma) \tag{54}$$

The density function for the normalized variable U is

$$f_U(x) = \frac{2}{\pi} \int_0^\infty d\omega \; R\left(\frac{\omega}{\sigma}\right) \cos \omega x, \; x \geq 0 \tag{55}$$

$$= \frac{2}{\pi} \int_0^\infty d\omega \; I\left(\frac{\omega}{\sigma}\right) \sin \; x, \; x \geq 0 \tag{56}$$

From this function various functions and moments pertaining to X can be calculated:

$$f_X(x) = \sigma^{-1} \; f_U(x \div \sigma) \tag{57}$$

$$F_X(x) = \int_0^{x \div \sigma} dy \; f_U(y) \tag{58}$$

$$m_n = \sigma^n \int_0^\infty dx \; f_U(y) x^n \tag{59}$$

Methods are also available for calculating $F_X(x)$ directly from the components of the characteristic function.*

Calculations for the normalized variable U require a value for σ. Means for its calculation or estimation are set forth below, as well as those for the mean value.

---

*Albert H. Nuttall, "Alternate Forms and Computational Considerations for Numerical Evaluation of Cumulative Probability Distributions Directly from Characteristic Functions," NUSC Report No. NL-3012, August 1970, Sec. 2.2.

The derivations are based on certain results given in BBN Report No. 3390; i.e., (2-21), (2-19), (2-20) and (2-22). These results are restated below for the first-order case in the same order. The cumulant function for X is

$$\psi_X(\omega) = \sum_{i=1}^{m} \sum_{j=1}^{n} \psi_{ij}(\omega) \tag{60}$$

The remaining equations are

$$\psi_{ij}(\omega) = \rho k_{ij} [H_{ij}(\omega) - H_{ij}(0)] \tag{61}$$

$$H_{ij}(\omega) = \int_{R_i} dg \int dq f_{Q_i}(q) \Phi_{S_j}(\omega z) \tag{62}$$

$$= \int_{R_i} dD \int dr |J(r,D)| f_{Q_i}(q) \Phi_{S_j}(\omega z) \tag{63}$$

where R_i is the area defined by the intersection of the sector with the i<u>th</u> route. The power transmission factor is implicitly a function of the position coordinates. The mean and the variance of X can be determined from the first and second derivatives of (60) evaluated at zero. This involves the first and second derivatives of (61), which in turn involves the first and second derivatives of (62) or (63).

To obtain results for direct calculations, differentiate (63) twice and evaluate for $\omega = 0$.

$$H'_{ij}(0) = \Phi'_{S_j}(0) \int dD \int_{R_i} dr\,|J(r,D)|\, f_{Q_i}(q)\, z(r,D) \qquad (64)$$

$$H''_{ij}(0) = \Phi''_{S_j}(0) \int dD \int_{R_i} dr\,|J(r,D)|\, f_{Q_i}(q)\, z^2(r,D) \qquad (65)$$

Substituting (64) and (65) into the corresponding derivatives of (60) and (61) gives expressions for $\psi'_X(0)$ and $\psi''_X(0)$. Exploiting the basic properties of cumulant and characteristic functions gives

$$m_X = \rho \sum_{i=1}^{m} \sum_{j=1}^{n} k_{ij} m_{S_j} \int dD \int_{R_i} dr\,|J(r,D)|\, f_{Q_i}(q)\, z(r,D) \qquad (66)$$

$$\sigma_X^2 = \rho \sum_{i=1}^{m} \sum_{j=1}^{n} k_{ij} (m_{S_j}^2 + \sigma_{S_j}^2) \int dD \int_{R_i} dr\,|J(r,D)|\, f_{Q_i}(q)\, z^2(r,D) \qquad (67)$$

where m_{S_j} is the average of the mean-squared pressure of sources of type j

$\sigma_{S_j}^2$ is the variance of the mean-squared pressure of sources of type j.

Each term of (66) or (67) can be regarded as an extension of Campbell's theorem*, which pertains to moments of elemental shot noise.

To obtain results for the approximations, differentiate (62) twice and evaluate for $\omega = 0$:

$$H'_{ij}(0) = \Phi'_{S_j}(0) \int dg \int_{R_i} dq f_{Q_i}(q) z(r,D) \tag{68}$$

$$H''_{ij}(0) = \Phi''_{S_j}(0) \int dg \int_{R_i} dq f_{Q_i}(q) z^2(r,D) \tag{69}$$

If the power transmission factor does not vary appreciably over R_i, then

$$z(r,D) \simeq z_i \tag{70}$$

where z_i is the power transmission factor from the reference point in R_i to the sensor.

If (70) is substituted in (68) and (69), the integrals can be readily evaluated, and the results are

*A. Papoulis, Probability, Random Variables, and Stochastic Processes, P. 359.

$$H'_{ij}(0) \simeq \Phi'_{S_j}(0)\,\ell_i z_i \tag{71}$$

$$H''_{ij}(0) \simeq \Phi''_{S_j}(0)\,\ell_i z_i^2 \tag{72}$$

where ℓ_i is the length of the route in R_i.

Substituting (71) and (72) into the corresponding derivatives of (60) and (61) gives approximate expressions for $\psi'_X(0)$ and $\psi''_X(0)$. Exploiting the basic properties of cumulant and characteristic functions gives

$$m_X \simeq \rho \sum_{i=1}^{m} \sum_{j=1}^{n} k_{ij} m_{S_j} \ell_i z_i \tag{73}$$

$$\sigma_X^2 \simeq \rho \sum_{i=1}^{m} \sum_{j=1}^{n} k_{ij} (m_{S_j}^2 + \sigma_{S_j}^2)\,\ell_i z_i^2 \tag{74}$$

The quantity $\rho k_{ij} \ell_i$ is the average number of ships of type j in R_i.

The problem of determining the points at which to calculate the characteristic function would be simple if the function were known in advance. If that were the case of course, there would be no need to calculate it. However, it will be possible to obtain an analytic approximation if (70) holds, and if the source characteristic function is analytic. Substituting (70) in (62) and evaluating the integrals gives

$$H_{ij}(\omega) = g_i \Phi_{S_j}(\omega z_i) \tag{75}$$

and substituting this result in (61) gives

$$\psi_{ij}(\omega) = \rho g_i k_{ij} [\Phi_{S_j}(\omega z_i) - 1] \tag{76}$$

Finally, substituting this result in (60) gives the cumulant function for X. However, it may not be necessary to do a complete evaluation. It appears from (76) that the critical routes are those with the larger power transmission factors z_i. Also, it might be that the source characteristic function for one class of ships has more detail than the others and necessitate more closely-spaced points ω_i. The result should be a good approximation for sector noise, but it will not be as accurate for beam noise.

3.2 An Inverse Fourier Transform Algorithm

The purpose of this section is to develop the equations for an approximation technique to evaluate the special form of the inverse Fourier transform given by (45) of Section 3.1:

$$f(x) = \frac{2}{\pi} \int_0^{+\infty} R(\omega) \cos\omega x \, dw, \tag{77}$$

for $x \geq 0$; where $f(x)$ is a probability density function such that $f(x) = 0$, for $x < 0$. $R(\omega)$ is the real part of the characteristic function of $f(x)$.

The first assumption is that $R(\omega)$ can be approximated by a quadratic in ω over a three-sample-point interval, that is

$$R(\omega) \simeq a\,\omega^2 + b\,\omega + c \tag{78}$$

for the general interval $\omega_n \leq \omega \leq \omega_{n+2}$. The constants a, b and c can be determined from the set of equations

$$\begin{aligned} R(n) &= a\,\omega_n^2 + b\,\omega_n + c \\ R(n+1) &= a\,\omega_{n+1}^2 + b\,\omega_{n+1} + c \\ R(n+2) &= a\,\omega_{n+2}^2 + b\,\omega_{n+2} + c \end{aligned} \tag{79}$$

where $R(n)$ is the value of the real part of the characteristic function at $\omega = \omega_n$, etc.

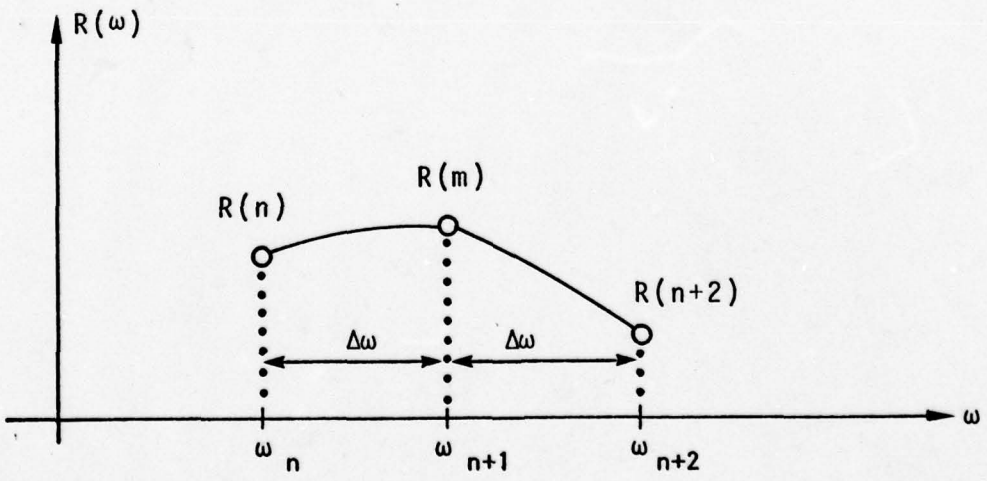

FIGURE 5 Approximating Polynomial

If it is also assumed that the samples are equally spaced in frequency ω, then

$$\omega_{n+2} = \omega_{n+1} + \Delta\omega = \omega_n + 2\,\Delta\omega \tag{80}$$

where $\Delta\omega$ is the interval between samples (See Figure 5.)

The solutions for the constants a, b and c in terms of $\Delta\omega$, R(n), R(n+1) and R(n+2) are given by

$$a = \frac{1}{2\Delta\omega^2}\quad [R(n) - 2R(n+1) + R(n+2)] \tag{81}$$

$$b = \frac{-1}{2\Delta\omega^2}\quad \Big\{ 2\omega_n\,[R(n) - 2R(n+1) + R(n+2)] + \Delta\omega\,[3R(n) - 4R(n+1) + R(n+2)]\Big\} \tag{82}$$

$$c = \frac{1}{2\Delta\omega^2}\quad \Big\{ R(n)\,(\omega_n + 2\,\Delta\omega)(\omega_n + \Delta\omega) - 2\omega_n\,R(n+1)(\omega_n + 2\,\Delta\omega) + \omega_n\,R(n+2)(\omega_n + \Delta\omega)\Big\} \tag{83}$$

Consider the inverse Fourier integral of Equation (77) evaluated over the general interval ω_n to ω_{n+2}, for some value of $x > 0$:

$$\Delta f_n(x) = \int_{\omega_n}^{\omega_{n+2}} R(\omega) \cos \omega x \, dw$$

Using the quadratic approximation for $R(\omega)$ given in Equation (78), we have

$$\Delta f_n(x) \cong \int_{\omega_n}^{\omega_{n+2}} [a\omega^2 + b\omega + c] \cos \omega x \, dw \qquad (84)$$

where the constants a, b and c are given in Equations (81) through (83). This integral can be evaluated exactly:

$$\Delta f_n(x) \cong \left[\frac{2a\omega + b}{x^2} \cos \omega x + \frac{(a\omega^2 + b\omega + c)x^2 - 2a}{x^3} \sin \omega x \right]_{\omega=\omega_n}^{\omega=\omega_{n+2}} \qquad (85)$$

Evaluating Equation (85) at the upper and lower limits and substituting the expressions for a, b and c from Equations (81) through (83) gives

$$\Delta f_n(x) \cong \frac{R(n) - 4R(n+1) + 3R(n+2)}{2\Delta\omega x^2} \cos \omega_{n+2} x$$

$$\cdot \frac{R(n+2)x^2 - \frac{1}{\Delta\omega^2}\left[R(n) - 2R(n+1) + R(n+2)\right]}{x^3} \sin \omega_{n+2} x$$

$$+ \frac{3R(n) - 4R(n+1) + R(n+2)}{2\Delta\omega x^2} \cos \omega_n x$$

$$- \frac{R(n)x^2 - \frac{1}{\Delta\omega^2}\left[R(n) - 2R(n+1) + R(n+2)\right]}{x^3} \sin \omega_n x \qquad (86)$$

The approximation for f(x) is equal to the sum of the contributions for each interval:

$$f(x) \cong \frac{2}{\pi} \sum_n \Delta f_n(x)$$

Assuming that the first sample point of the real part of the characteristic function R(0) is at $\omega = 0$, and the last point R(N) is at $\omega = \omega_N$, there will be a total of N + 1 sample points. The number (N + 1) must be an odd integer, for example, 3, 5, 7, 9, etc. Figure 6 shows the sampling scheme.

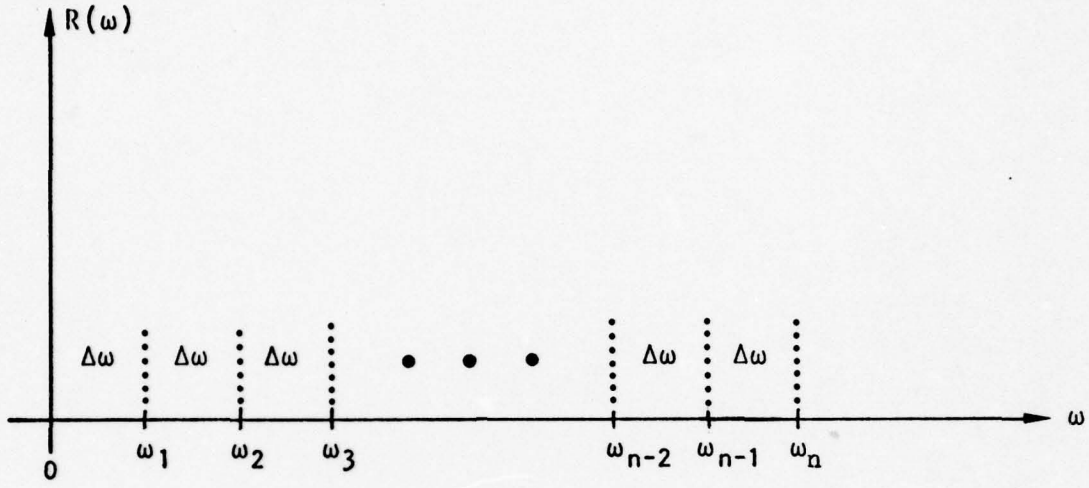

FIGURE 6 Sampling Scheme

With these assumptions, the approximation for f(x) can be simplified after considerable algebraic manipulation

$$f(x) \cong \frac{3R(0) - 4R(1) + R(2)}{\pi \Delta\omega\, x^2}$$

$$+ \frac{1}{\pi \Delta\omega\, x^2} \sum_{n=2}^{N-2} \left\{ \left[R(n-2) - 4R(n-1) + 6R(n) - 4R(n+1) + R(n+2) \right] \cos\omega_n x \right.$$

(n goes by steps of 2)

$$- \frac{2R(n-2) - 4R(n-1) + 4R(n+1) - 2R(n+2)}{\Delta\omega x} \sin \omega_n x \Bigg\}$$

$$+ \frac{R(N-2) - 4R(N-1) + 3R(N)}{\pi\Delta\omega\, x^2} \cos \omega_N x$$

$$+ \frac{2R(N)x^2 - \frac{2}{\Delta\omega^2}[R(N-2) - 2R(N-1) + R(N)]}{\pi x^3} \sin \omega_N x$$

for $x > 0$

(87)

A recursion relationship can be derived for $\sin \omega_n x$ and $\cos \omega_n x$ because of the equal spacing of samples in the frequency domain. Note that $\omega_n = n\Delta\omega$, where $\Delta\omega$ is the interval between samples. Therefore,

$$\sin \omega_n x = \sin n\Delta\omega x$$

$$= 2 \sin (n-1)\Delta\omega x \cos \Delta\omega x - \sin (n-2)\Delta\omega x \quad (88)$$

The recursion relation becomes

$$\sin \omega_n x = [2 \cos \Delta\omega x] \sin \omega_{n-1} x - \sin \omega_{n-2} x \qquad (89)$$

The first three values are

$$\sin \omega_o x = 0$$

$$\sin \omega_1 x = \sin \Delta\omega x$$

$$\sin \omega_2 x = [2 \cos \Delta\omega x] \sin \Delta\omega x$$

The recursion relationship for $\cos \omega_n x$ is

$$\cos \omega_n x = [2 \cos \Delta\omega x] \cos \omega_{n-1} x - \cos \omega_{n-2} x \qquad (90)$$

The first three values are

$$\cos \omega_o x = 1$$

$$\cos \omega_1 x = \cos \Delta\omega x$$

$$\cos \omega_2 x = 2[\cos \Delta\omega x]^2 - 1$$

The numerical approximation formula for f(x) given by Equation (87) is valid for any $x > 0$. For the case where $x = 0$, we must use a different formula. From Equation (77) we have

$$f(0) = \frac{2}{\pi} \int_0^{+\infty} R(\omega)\, d\omega \qquad (91)$$

Using the quadratic approximation for $R(\omega)$ given by Equations (78) and (81) in Equation (91), $f(0)$ is approximately equal to

$$f(0) \cong \frac{2\Delta\omega}{3\pi} [R(N) - R(0)] + \frac{4\Delta\omega}{3\pi} \sum_{n=0}^{N-2} [R(n) + 2R(n+1)] \qquad (92)$$

(n goes by steps of 2; i.e., n = 0, 2, 4, 6, etc.)

4.0 PROGRAM INPUTS

The prediction of the beam noise density function requires acoustic data pertaining to the sensor, its acoustic basin, and surface ships. Section 4.1 discusses a beam pattern function for a shaded line array of hydrophones. Section 4.2 gives route geometry data for the Northeast Pacific Ocean, and Section 4.3 presents required source characteristic functions for classes of surface ships.

4.1 Beam Pattern Function

In the calculations described in Reference 1, only the noise in a narrow sector due to merchant shipping was considered. For the present effort, the entire beam pattern is to be incorporated into the calculations. The approach given in the sequel is to use the normalized beam pattern as a weighting coefficient to be applied for a given angle in the calculations Φ_Y.

Engineers of the Naval Research Laboratory supplied a beam pattern approximating Hanning shading:

$$B(\theta) = \left[\frac{N}{2} \frac{\sin \pi\beta}{\pi\beta \ (1-\beta^2)} \right]^2 \qquad (93)$$

where

$$\beta = \frac{L}{\lambda} (\sin \theta - \sin \theta_s)$$

and

θ_s = beam steered direction

θ = angle from broadside

L = length of the array

N = number of phones

λ = c/f

c = speed of sound

f = frequency

Figure 7 shows the reference for the array angles.

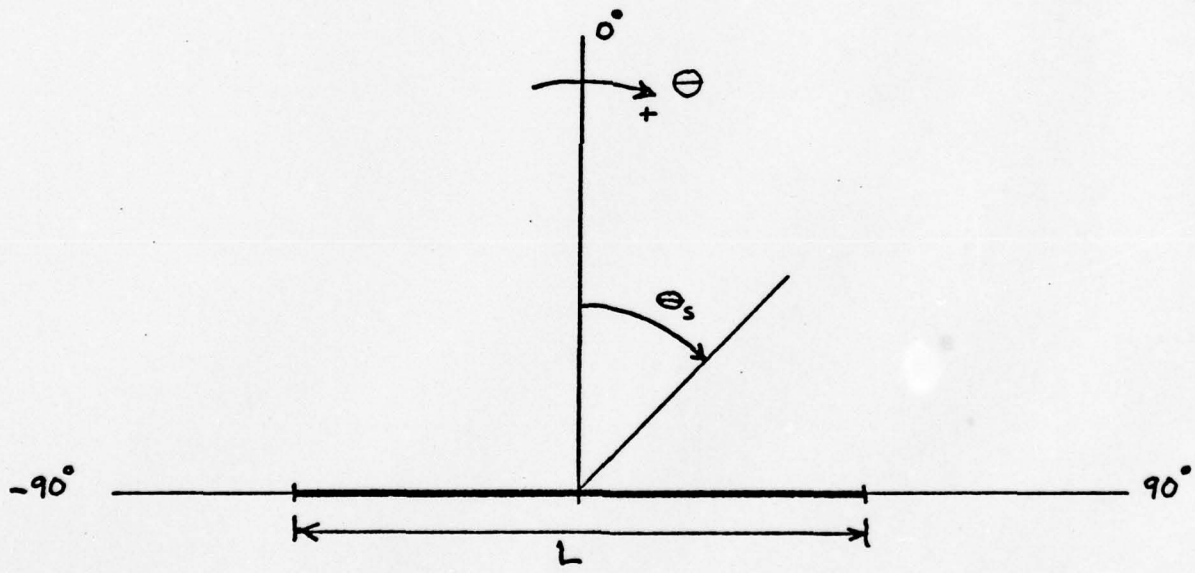

FIGURE 7 Array Angles

Let f_o equal the design frequency and c_o equal the design value of the speed of sound. The phone spacing d is given by

$$d = \frac{\lambda_o}{2} = \frac{c_o}{2f_o} \tag{94}$$

The length of the array L is given by

$$L = (N-1)d = (N-1)\frac{c_o}{2f_o} \tag{95}$$

Define the constant $\alpha \triangleq \frac{L}{\lambda}$. Therefore,

$$\alpha = \frac{(N-1)}{2}\frac{c_o f}{c f_o} \tag{96}$$

Table 2 gives the value of α for four selected frequencies. A design speed of sound c_o = 5,000 ft./sec. and an actual speed of sound of c = 4,860 ft./sec. were used in the computation of α.

Table 2: Values of α for Four Frequencies

f(Hz)	f_o(Hz)	N	α
10	20	62	15.68930041
40	60	58	19.5473251
50	60	58	24.43415638
300	320	64	30.38194444

The normalized beam pattern BP is given by

$$BP = \left[\frac{\sin \pi\beta}{\pi\beta \ (1-\beta^2)} \right]^2 \tag{97}$$

where $\beta = \alpha \ (\sin \theta - \sin \theta_s)$.

Note that there are three points ($\beta = 0$ and $\beta = \pm 1$) at which the function is an indeterminate form. Using L'Hospital's rule BP can be evaluated at these points

$$BP = 1.0 \text{ at } \beta = 0 \tag{98}$$

and

$$BP = 0.25 \text{ at } \beta = \pm 1 \tag{99}$$

Figure 8 shows the normalized beam pattern, converted to dB for a frequency of 10 Hz and a steering angle θ_s of -9 degrees (351°).

Figure 9 shows the normalized beam pattern, converted to dB for a frequency of 50 Hz and θ_s = -9 degrees. Note that as the frequency increases, the main lobe becomes narrower and there are more side lobes.

In the computations of the characteristic function for Y, there is an integral over the angle D. The step size for this intergral will have to be adjusted such that the time for computation on the digital computer is not excessive. One approach is to use a finer step size for angles in the main lobe, and a coarser step size for angles in the side lobes. However, for

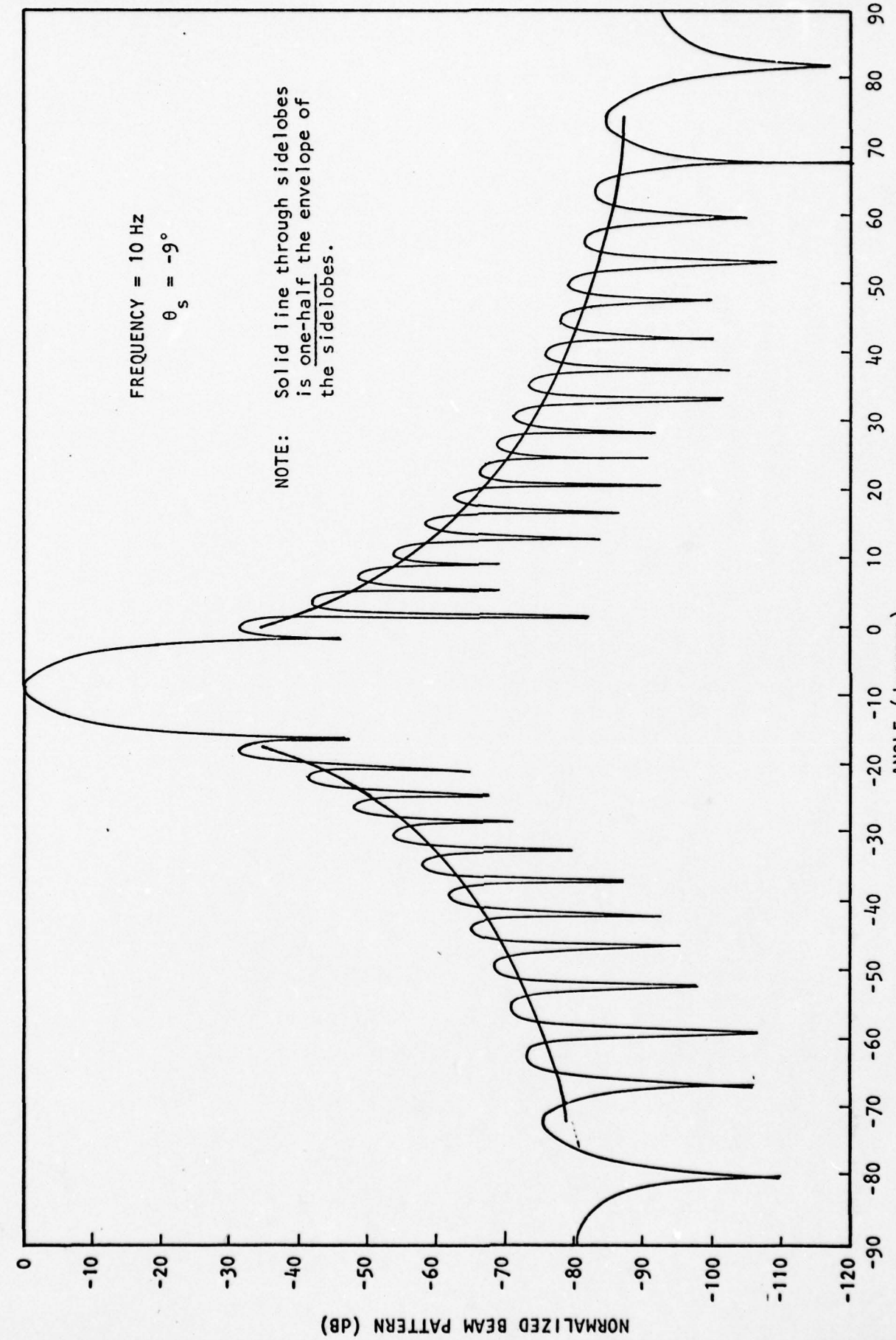

FIGURE 8 Beam Pattern for 10 Hz.

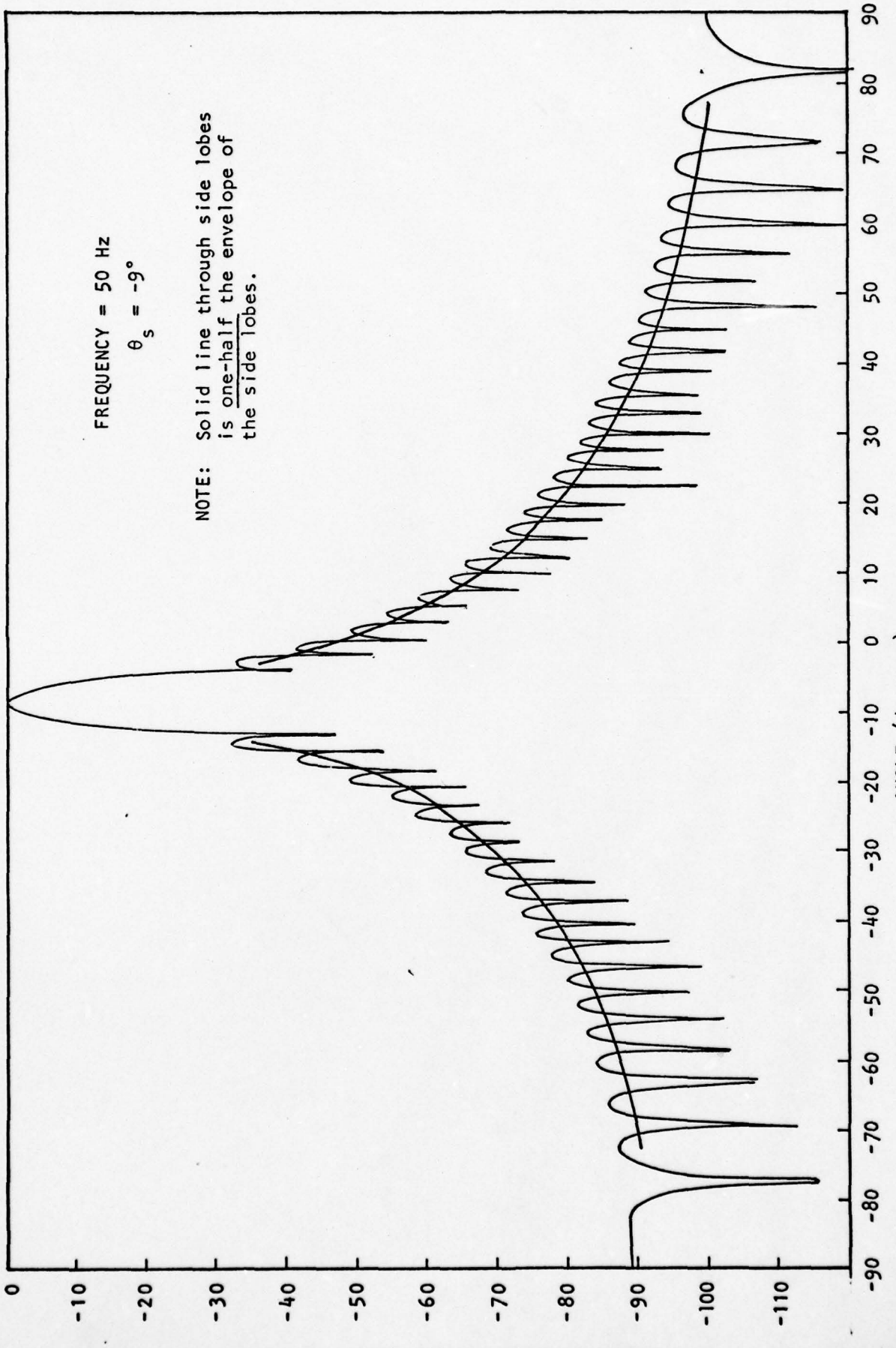

FIGURE 9 Beam Pattern for 50 Hz.

the side lobes an approximation must be used that is compatible with coarser angle step sizes. For the side lobes, the normalized beam pattern will be modelled as one-half the envelope value, that is

$$BP = 1/2 \left[\frac{1}{\pi\beta\,(1-\beta^2)}\right]^2 \qquad (100)$$

Note that the main lobe occurs for $-2 \leq \beta \leq +2$ and the side lobes occur for values of β outside this range.

In Figures 8 and 9 the one-half envelope approximation is shown as the solid line through the side lobes.

4.2 Route Geometry Data for Northeast Pacific Ocean

This section sets forth route data for the Northeast Pacific Ocean.

Eight routes were selected from the seventy-five canonical routes described in Reference 5. However, in some instances, portions of the canonical routes are eliminated because it is felt that they contribute little to the noise statistics. For example, it is felt that the Aleutian chain forms an effective boundary for the Northern Pacific; therefore, the canonical route from Honolulu to Nome is terminated at the Unimak Pass. Further, due to internal constraints of the program module GEOM*, two of these eight routes must be counted as double routes. Therefore, the example contains, in effect, ten routes.

*Described in Section VII of Reference 6.

Each route consists of one or more segments, with the following items needed for each segment:

1. latitude and longitude of the end-points
2. width at the end-points
3. maximum width
4. ship densities for each class of vessel

Table 3 contains Items 1, 2 and 3 for each of the ten routes considered in this case. Route and segment numbers are descriptors used by the program GEOM. In addition, geographic designations are given for each segment end-point. Figure 10 is a map of the Pacific Ocean, indicating (approximately) the positions of the routes.

4.3 Source Characteristic Functions

It is shown in Section 2.1 that the calculation of the characteristic function of Y requires a source characteristic function $\Phi_{SJ}(\ )$ for each type of ship. In particular, each of these characteristic functions pertains to the same frequency band as the ambient noise prediction.

The required source characteristic functions were derived from statistical information produced by Heine and Gray [3] pertaining to principal sources of noise radiated by merchant ships. This information was employed to derive discontinuous probability density functions for the level of each type of source.

ROUTE NUMBER	NUMBER OF SEGMENTS	SEGMENT NUMBER	SEGMENT ORIGIN			SEGMENT TERMINUS			SEGMENT MAXIMUM WIDTH (Degrees)
			LATITUDE LONGITUDE	SEGMENT WIDTH (Degrees)	GEOGRAPHIC DESIGNATION	LATITUDE LONGITUDE	SEGMENT WIDTH (Degrees)	GEOGRAPHIC DESIGNATION	
1	2	1	45°43'N 142°40'E	.25	La Perouse Strait (East End)	54°20'N 165° 0'W	.125	Unimak Pass	4.0
		2	54°20'N 165°40'W	.125	Unimak Pass	48°30'N 124°40'W	0.0	Strait of Juan De Fuca	4.0
2	4	1	35°27'N 139°39'E	0.0	Yokohoma	43° 0'N 150° 0'E	2.0	Mid-Ocean	3.0
		2	43° 0'N 150° 0'E	2.0	Mid-Ocean	43° 0'N 170° 0'W	0.0	Mid-Ocean	3.0
		3	43° 0'N 170° 0'W	0.0	Mid-Ocean	43° 0'N 160° 0'W	4.0	Mid-Ocean	4.0
		4	43° 0'N 160° 0'W	4.0	Mid-Ocean	48°30'N 124°40'W	0.0	Strait of Juan De Fuca	4.0
3	1	1	43° 0'N 160° 0'W	4.0	Mid-Ocean	37°48'N 122°24'W	0.0	San Francisco	4.0
4	1	1	21°40'N 157°30'W	0.0	Honolulu	54°20'N 165° 0'W	.125	Unimak Pass	4.0
5	1	1	21°40'N 157°30'W	0.0	Honolulu	48°30'N 124°40'W	0.0	Strait of Juan De Fuca	4.0
6	1	1	21°40'N 157°30'W	0.0	Honolulu	37°35'N 122°40'W	0.0	San Francisco	4.0
7	1	1	6°55'N 81°25'W	.3333	Isla Coiba	21°30'N 157°35'W	0.0	Honolulu	4.0
8	1	1	37°48'N 122°24'W	0.0	San Francisco	17°32'S 149°34'W	0.0	Papeete	4.0
9	1	1	54°20'N 165° 0'W	0.0	Unimak Pass	48°30'N 124°40'W	0.0	Strait of Juan De Fuca	3.0
10	2	1	48°30'N 124°40'W	0.0	Strait of Juan De Fuca	40°18'N 124°30'W	1.0	Cape Medocino	1.5
		2	40°18'N 124°30'W	1.0	Cape Mendocino	37°48'N 122°24'W	0.0	San Francisco	1.0

TABLE 3 ROUTE / SEGMENT GEOMETRIC DATA.

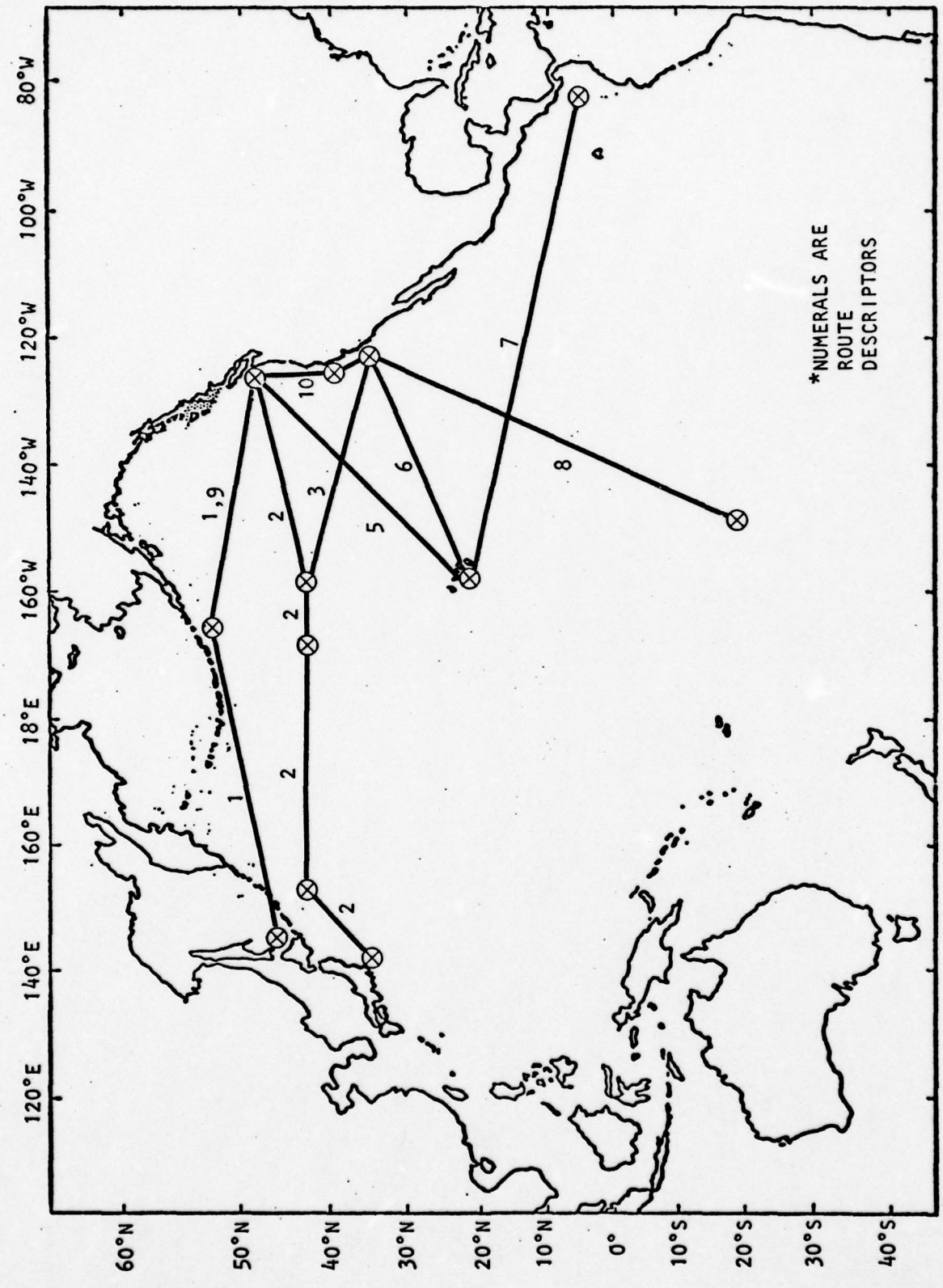

FIGURE 10 Route / Segment Geometry

The procedure for obtaining the source characteristic function from the discontinuous density functions is outlined below.

1. Select a characteristic function with at least two parameters that applies to a non-negative random variable.

2. Calculate the low-order moments of the source intensity of each component. These can be readily obtained from the discontinuous density functions $f_{U_k}(\ )$ for the component source levels. For example, the mean value of the source intensity of the $i^{\underline{th}}$ component is

$$m_i = \int du\ 10^{u \div 10}\ f_{Ui}(u) \qquad (101)$$

3. Determine the low-order moments of the source intensity from the low-order moments of the component source intensities.

4. Determine the values of the parameters of the characteristic function so that its moments match the calculated moments.

The advantage of this procedure is that it avoids the excessive oscillations of the characteristic functions that would be introduced by the direct utilization of the discontinuous density functions.

The remainder of this section (1) summarizes the information developed by Heine and Gray, (2) presents plots of the probability density functions derived from them, and (3) gives the low-order moments of the source intensity derived from the source level density functions.

Heine and Gray developed histograms for the source level and frequency for four categories of radiated noise. The spectral components considered were a broadband component due to propeller cavitation; lines at the propeller blade rate and harmonics; lines at the diesel firing rate and harmonics; and a line at the electric plant frequency. The histograms pertain to "Long Range Effective Source Level" (LRESL), defined as [3] the power radiated by an omnidirectional source (at a depth of 20 feet) between depression angles zero and fifteen degrees (including that from surface interference).

4.3.1 Broadband Cavitation

Heine and Gray found it useful to divide the merchant fleet into three classes of vessel-fishing, small merchant, and large merchant. In addition, each of these was divided into eight acoustic classes. Histograms showing the distribution of acoustic class for each class of vessel are shown in Figures 11, 12 and 13, while their broadband spectra are shown in Figure 14.

Assuming statistical independence between the acoustic class and broadband spectrum, composite histograms are formed for the source level at the frequencies 10, 40, 50 and 300 Hz (in a 1-Hz band), for the three classes of vessel. Finally, by considering 10 dB increments and normalizing the area to unity, an approximate probability density function is generated

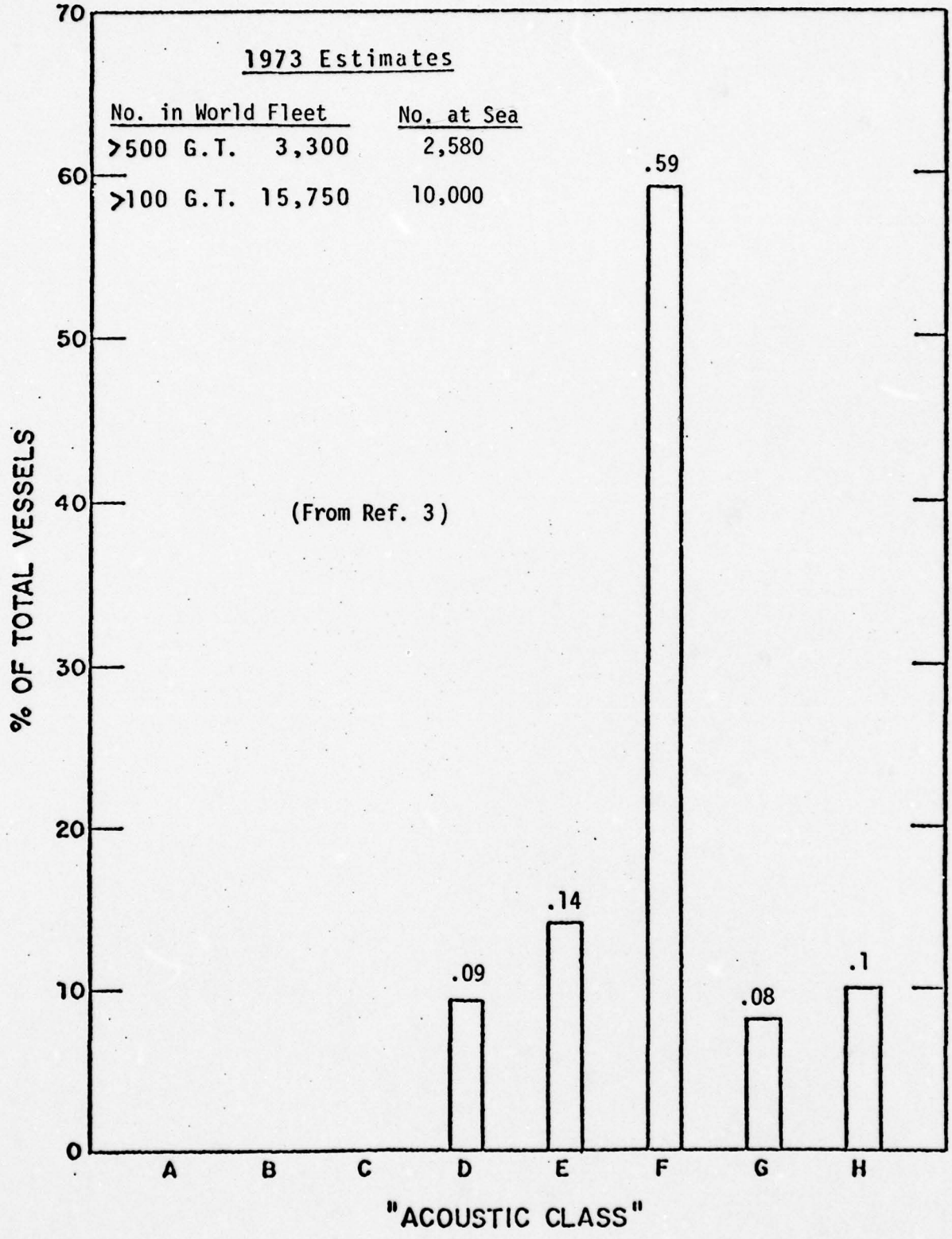

FIGURE 11 Distribution of Broadband Classes, Fishing Vessels

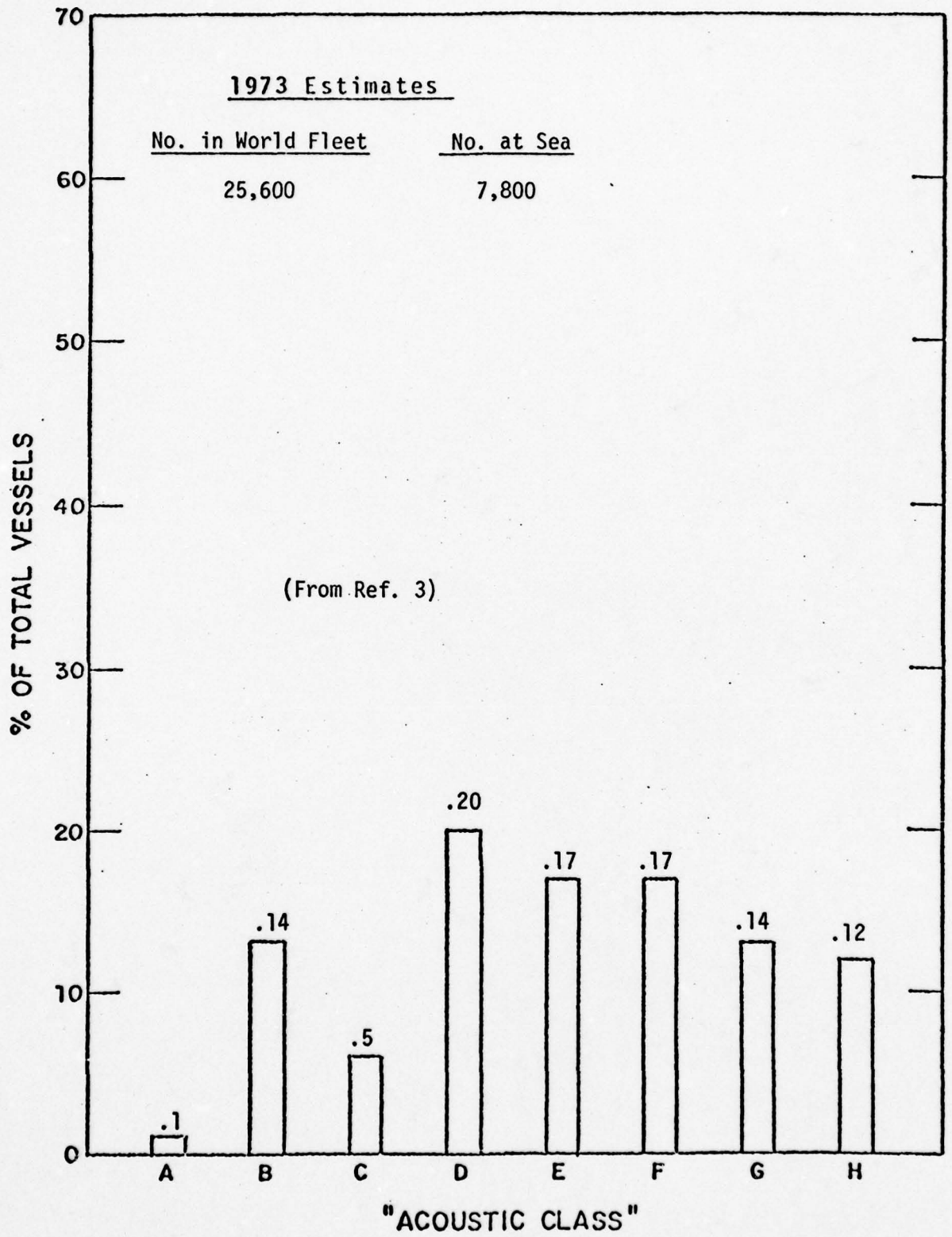

FIGURE 12 Distribution of Broadband Classes, Merchant Vessels Less than 700 Feet LOA

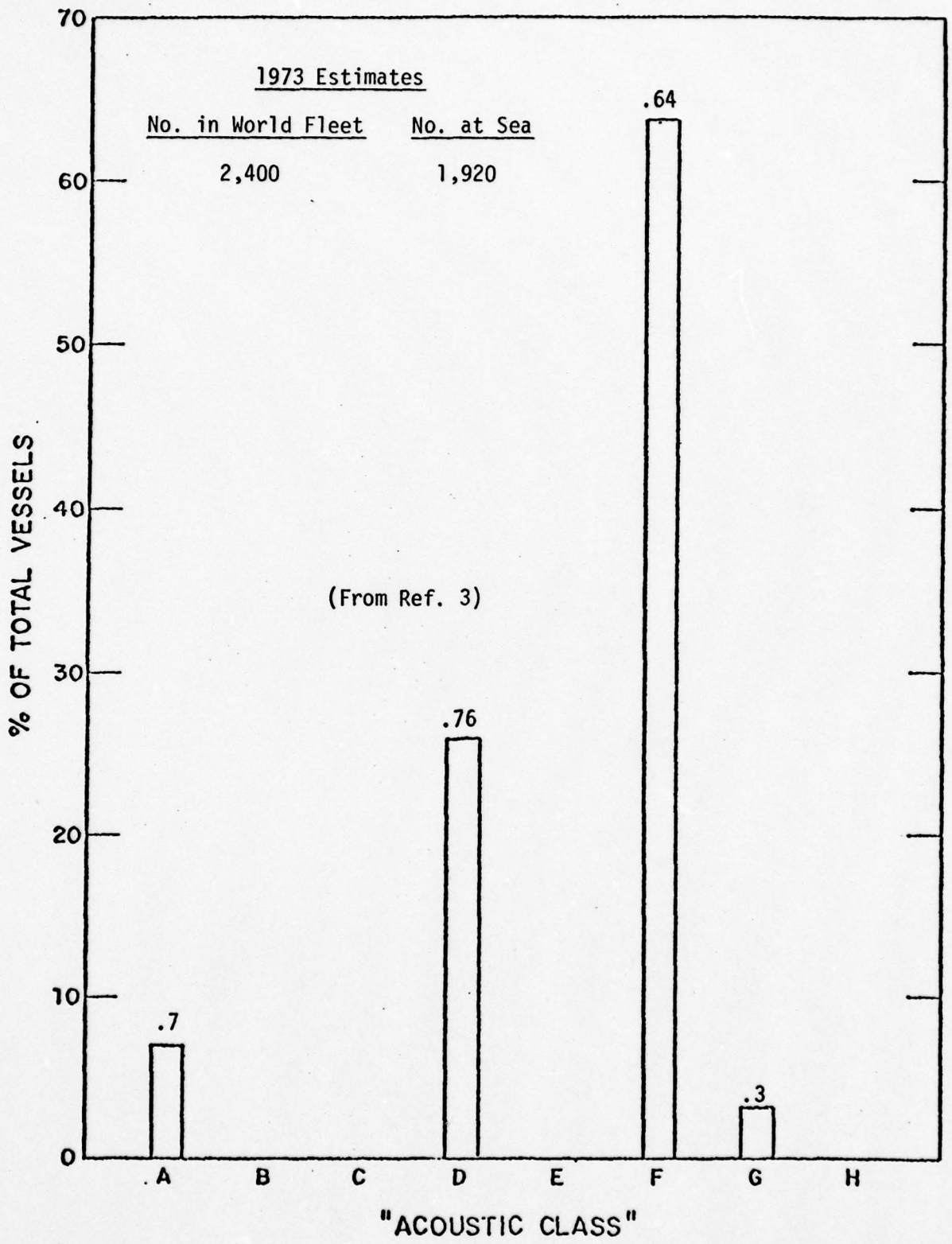

FIGURE 13 Distribution of Broadband Classes, Merchant Vessels Greater than 700 Feet LOA

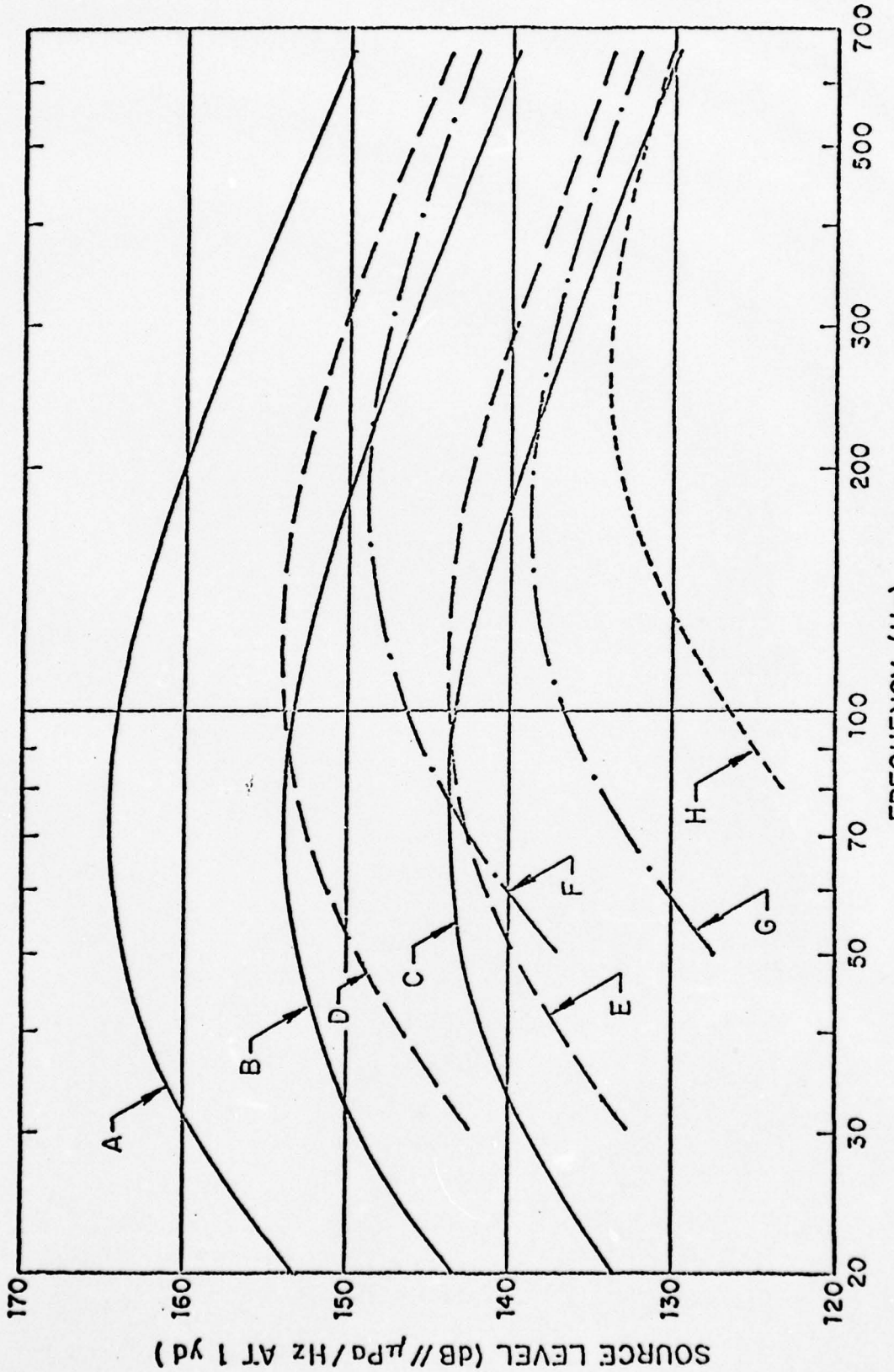

FIGURE 14 Broadband Acoustic Class Spectra

from each composite histogram. These density functions are shown in Figures 15 through 26

4.3.2 Propeller Blade Rate and Harmonics

Heine and Gray [3] developed histograms for the source level and the fundamental frequency for the three classes of vessel. Gray [6] modified the source level distribution and developed a [7] model for the effects of harmonics.

Assuming statistical independence between source level and frequency, probability density functions were generated for source level at the frequencies 10, 40, 50 and 300 Hz (in a .2-Hz band) for the three classes of vessel. These distributions include the effects of the first nine harmonics. Note that fishing vessels contribute nothing at 10 Hz, while small and large merchant contribute nothing at 300 Hz. These monopole source level density functions are shown in Figures 27 through 35. The figures give values for $P(-\infty)$, which is the probability that there is no line in the specified 1-Hz band. The procedure employed is described in Section 4.2 of Reference 1.

4.3.3 Electric Plant Frequency

Heine and Gray [3] developed histograms for the source level and frequency for the three classes of vessel. Assuming statistical independence again, a probability density function was generated for the source level at 50 Hz for each class of vessel. Since the frequencies that are of interest are 10, 40, 50 and 300 Hz, the line at 60 Hz does not contribute any power. The probability density functions are shown in Figures 36, 37 and 38.

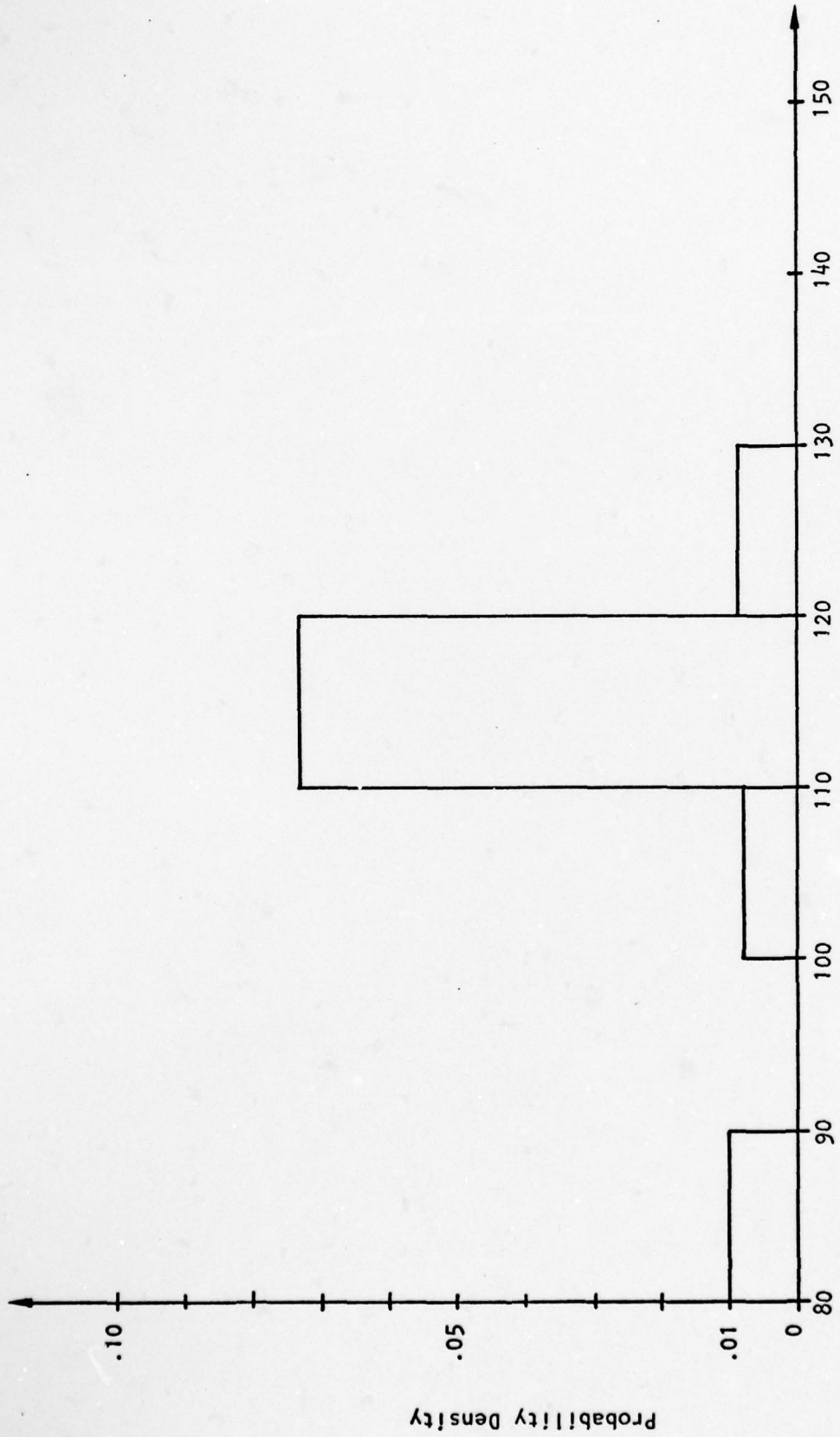

FIGURE 15 Broadband Source Level Distribution for Fishing Vessels at 10 Hz.

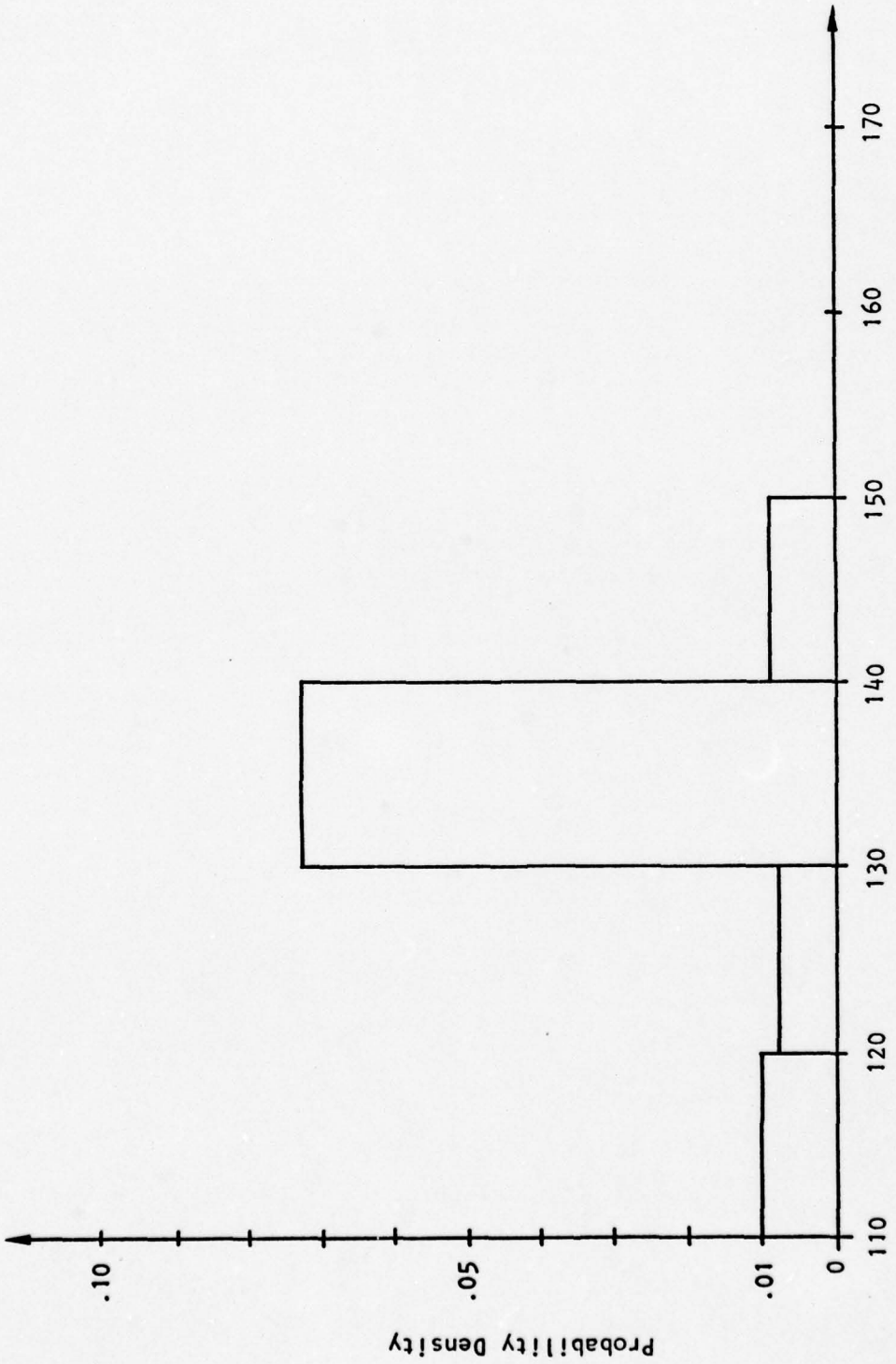

FIGURE 16 Broadband Source Level Distribution for Fishing Vessels at 40 Hz.

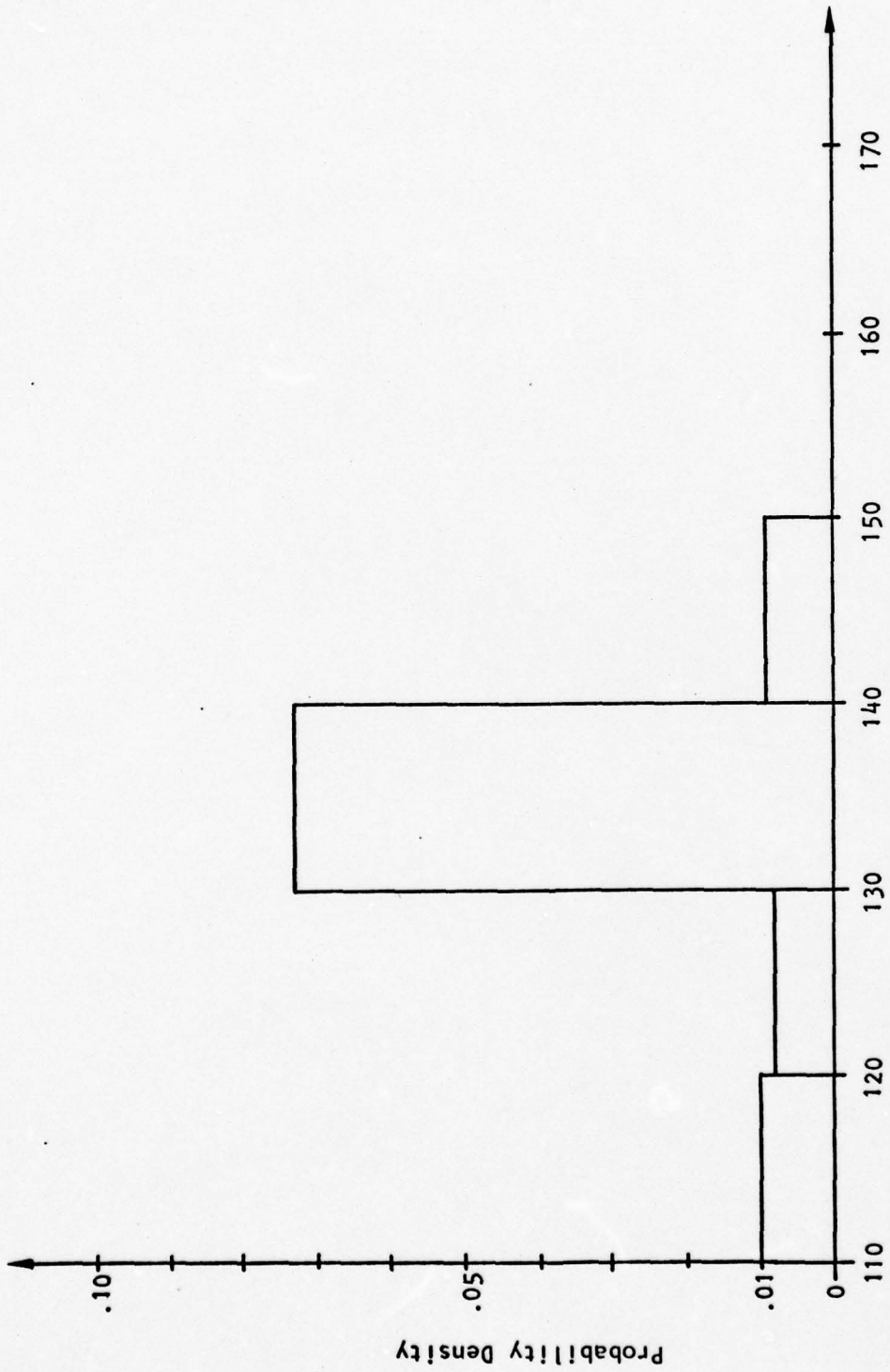

FIGURE 17 Broadband Source Level Distribution for Fishing Vessels at 50 Hz.

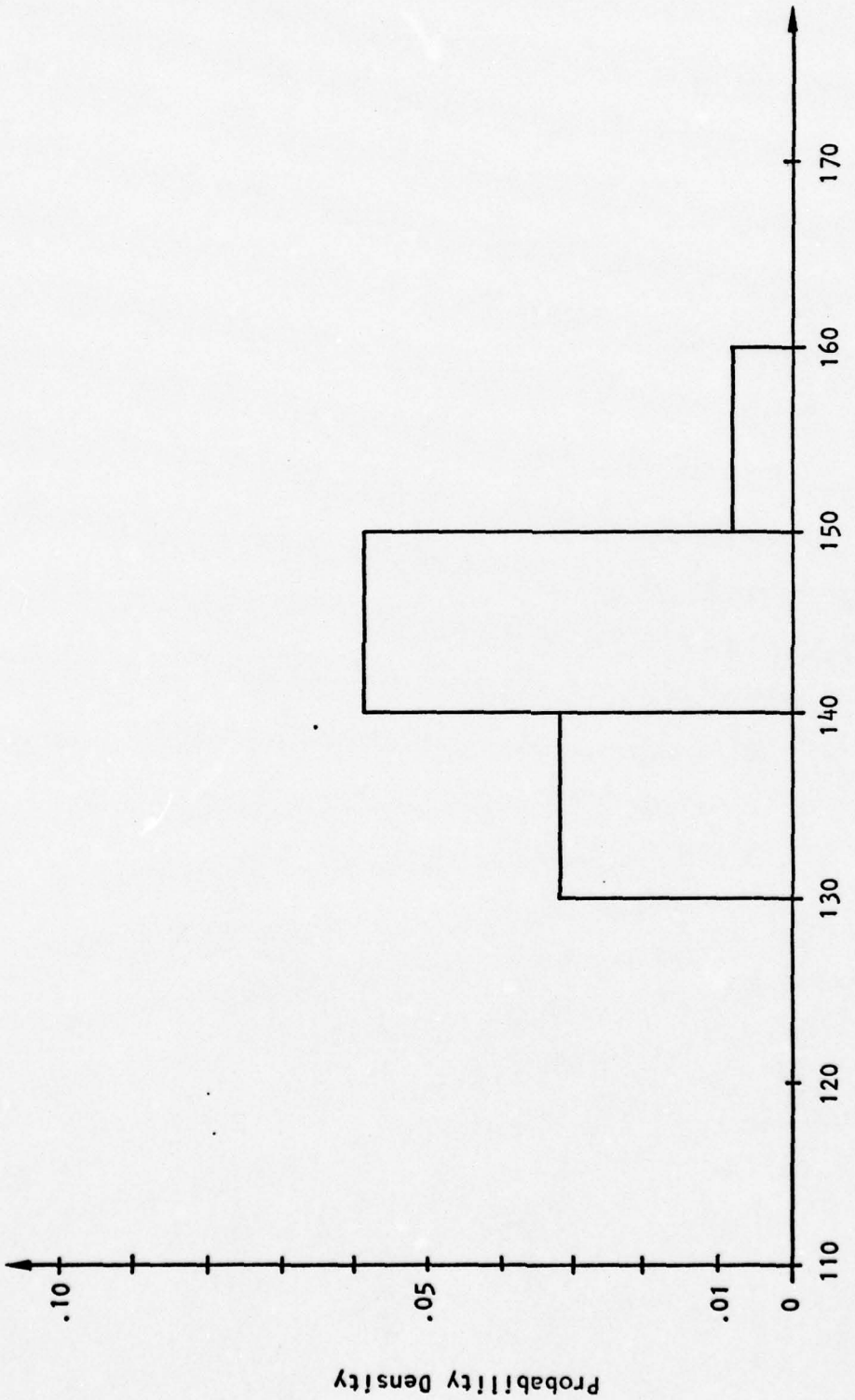

FIGURE 18 Broadband Source Level Distribution for Fishing Vessels at 300 Hz.

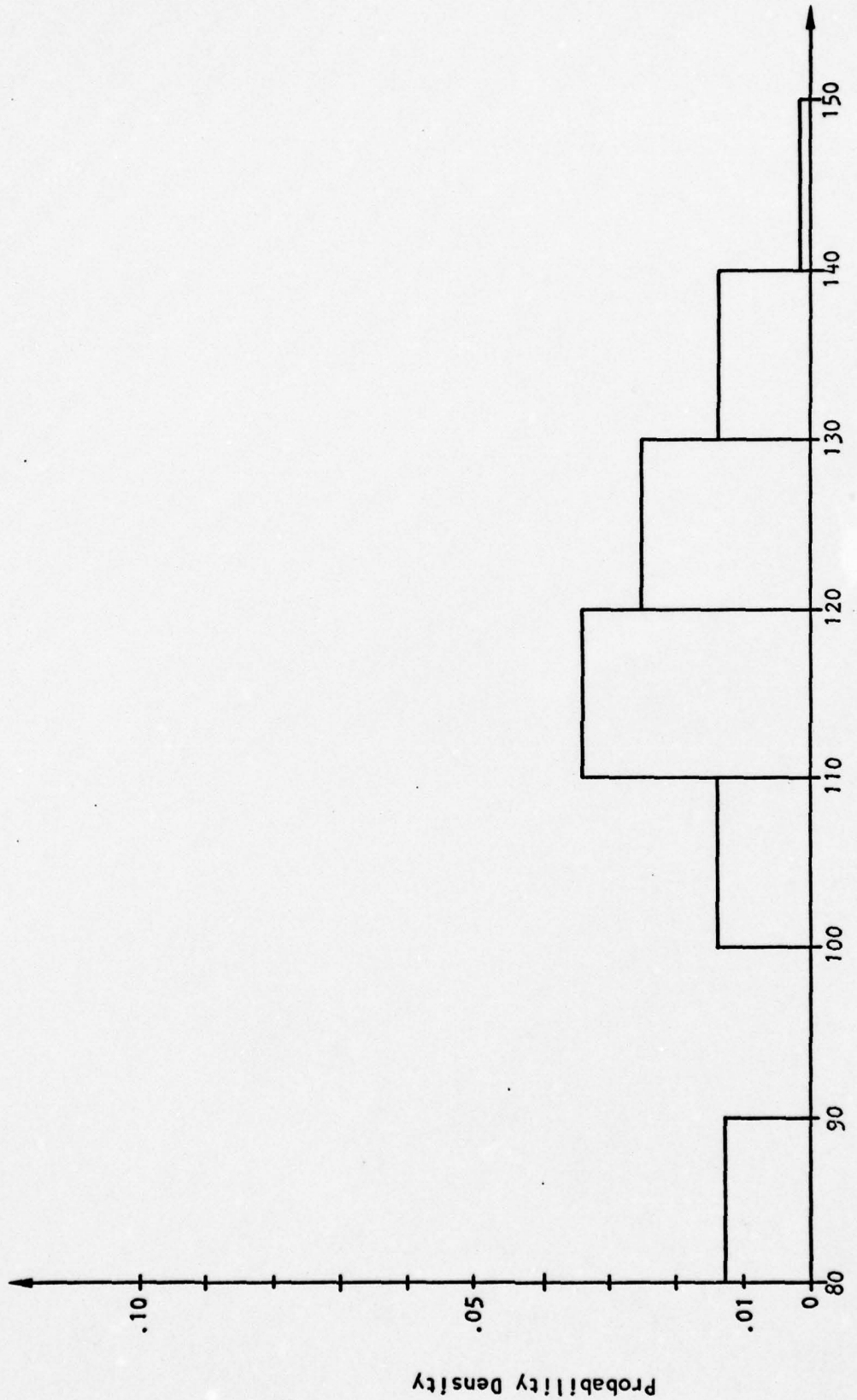

FIGURE 19 Broadband Source Level Distribution for Small Merchant Ships at 10 Hz.

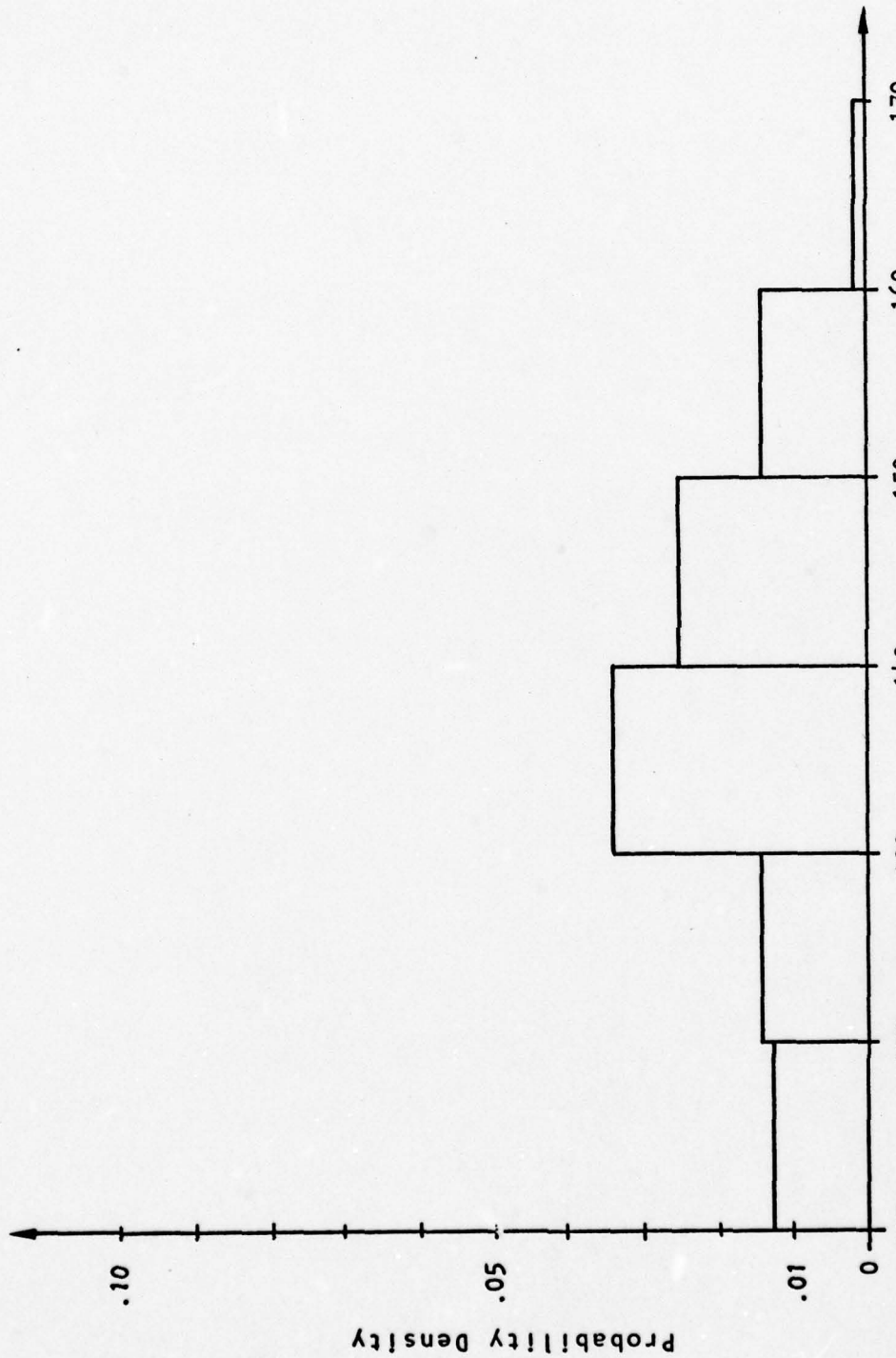

FIGURE 20 Broadband Source Level Distribution for Small Merchant Ships at 40 Hz.

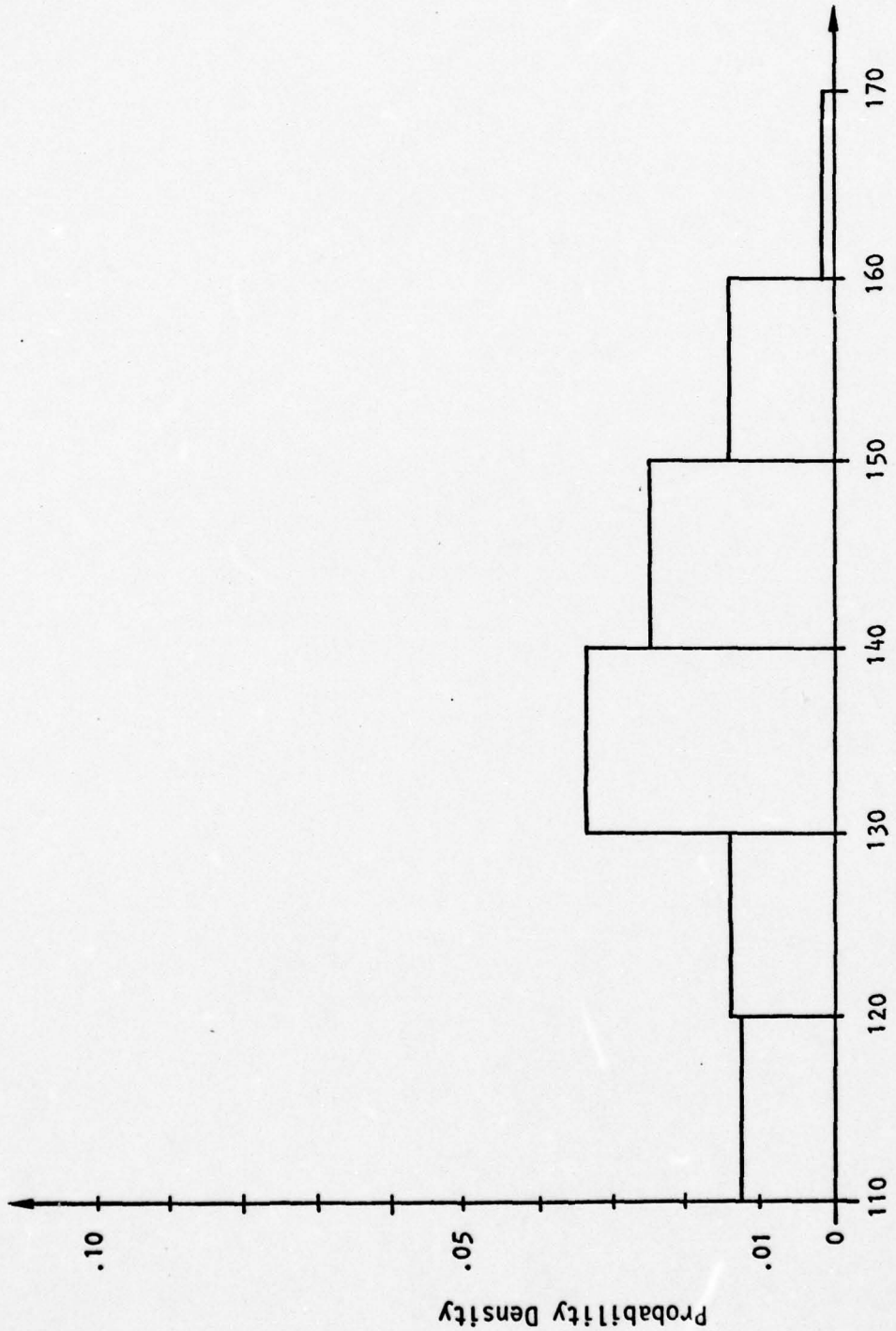

FIGURE 21 Broadband Source Level Distribution for Small Merchant Ships at 50 Hz.

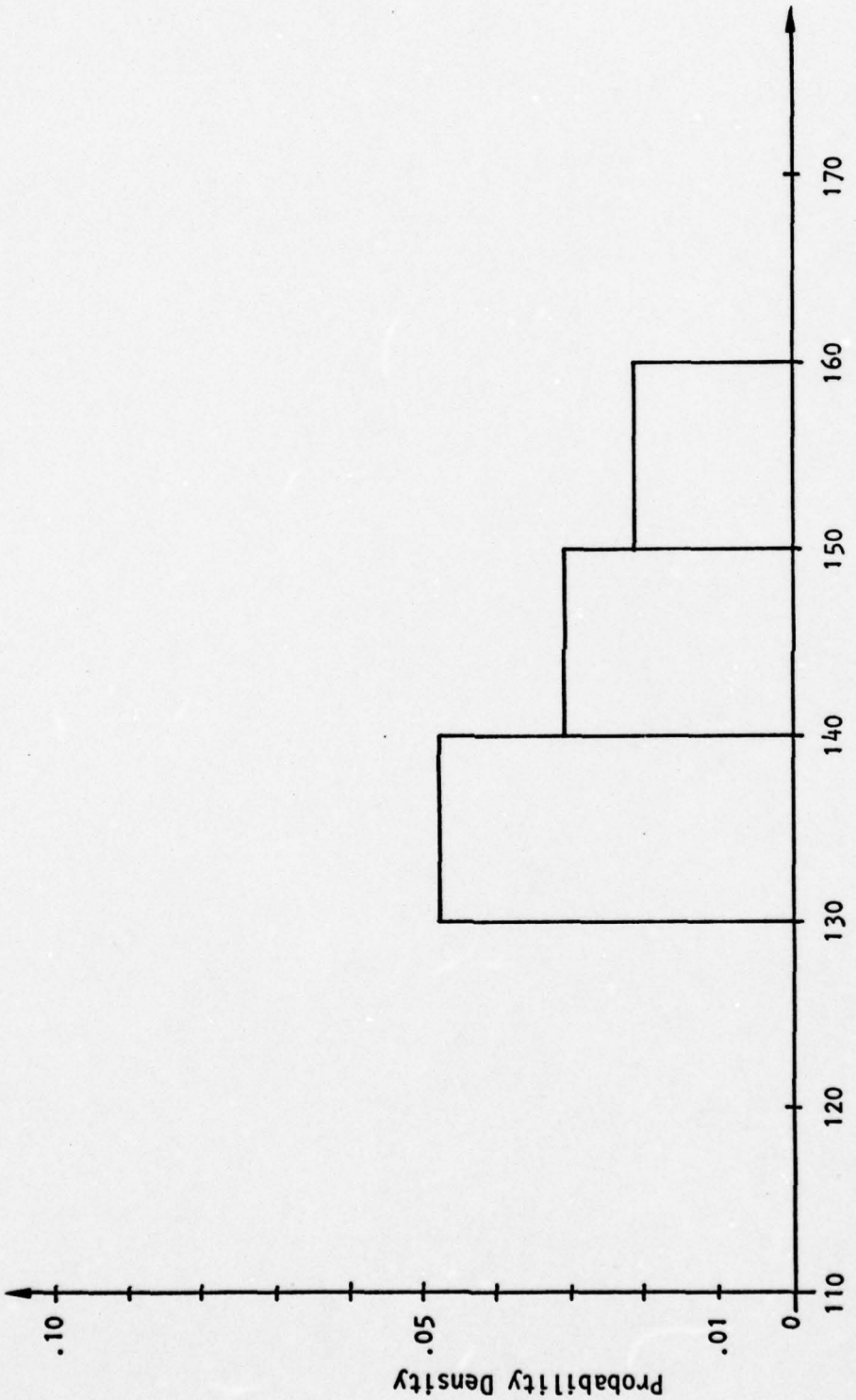

FIGURE 22 Broadband Source Level Distribution for Small Merchant Ships at 300 Hz.

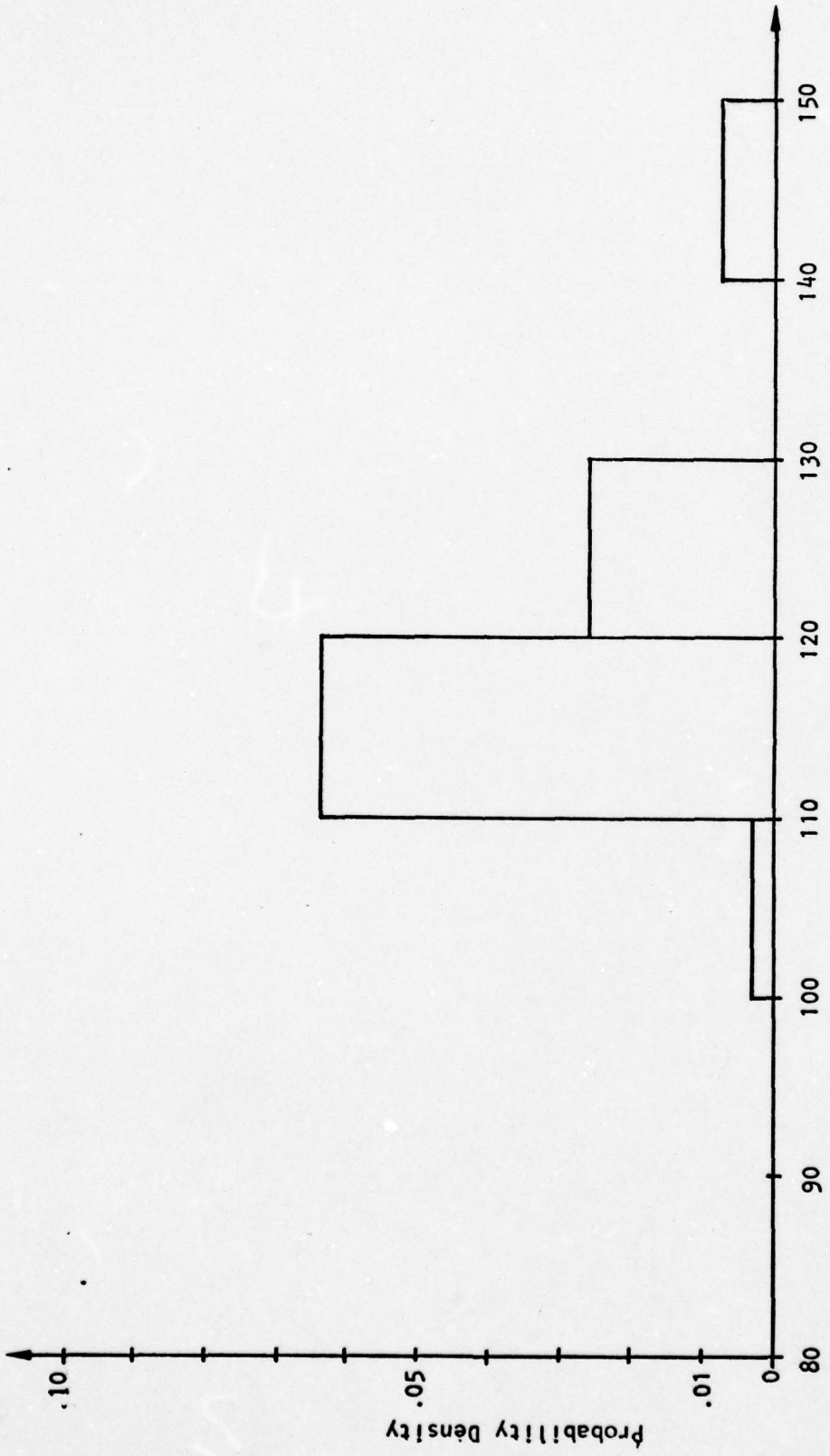

FIGURE 23 Broadband Source Level Distribution for Large Merchant Ships at 10 Hz.

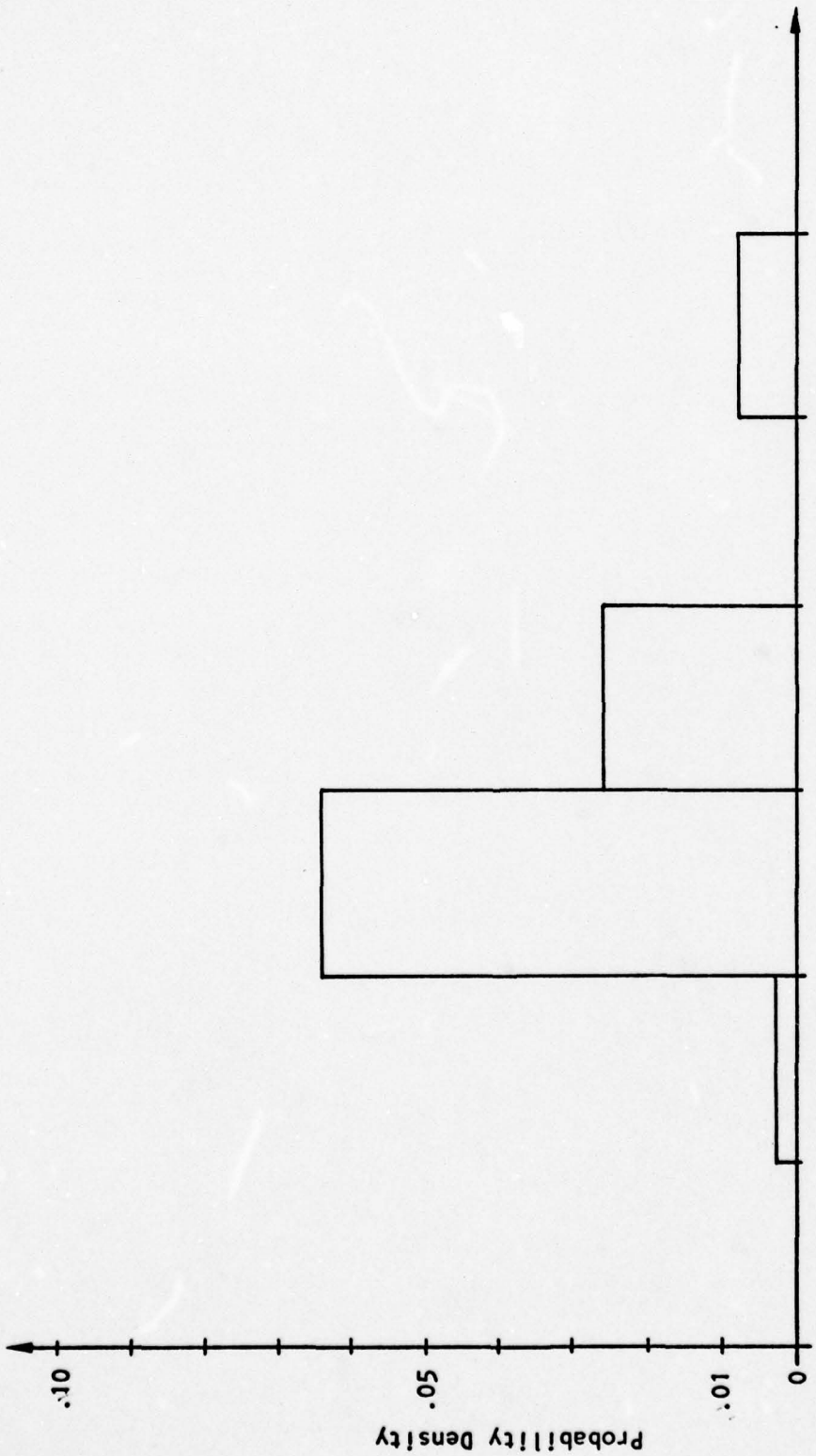

FIGURE 24 Broadband Source Level Distribution for Large Merchant Ships at 10 Hz.

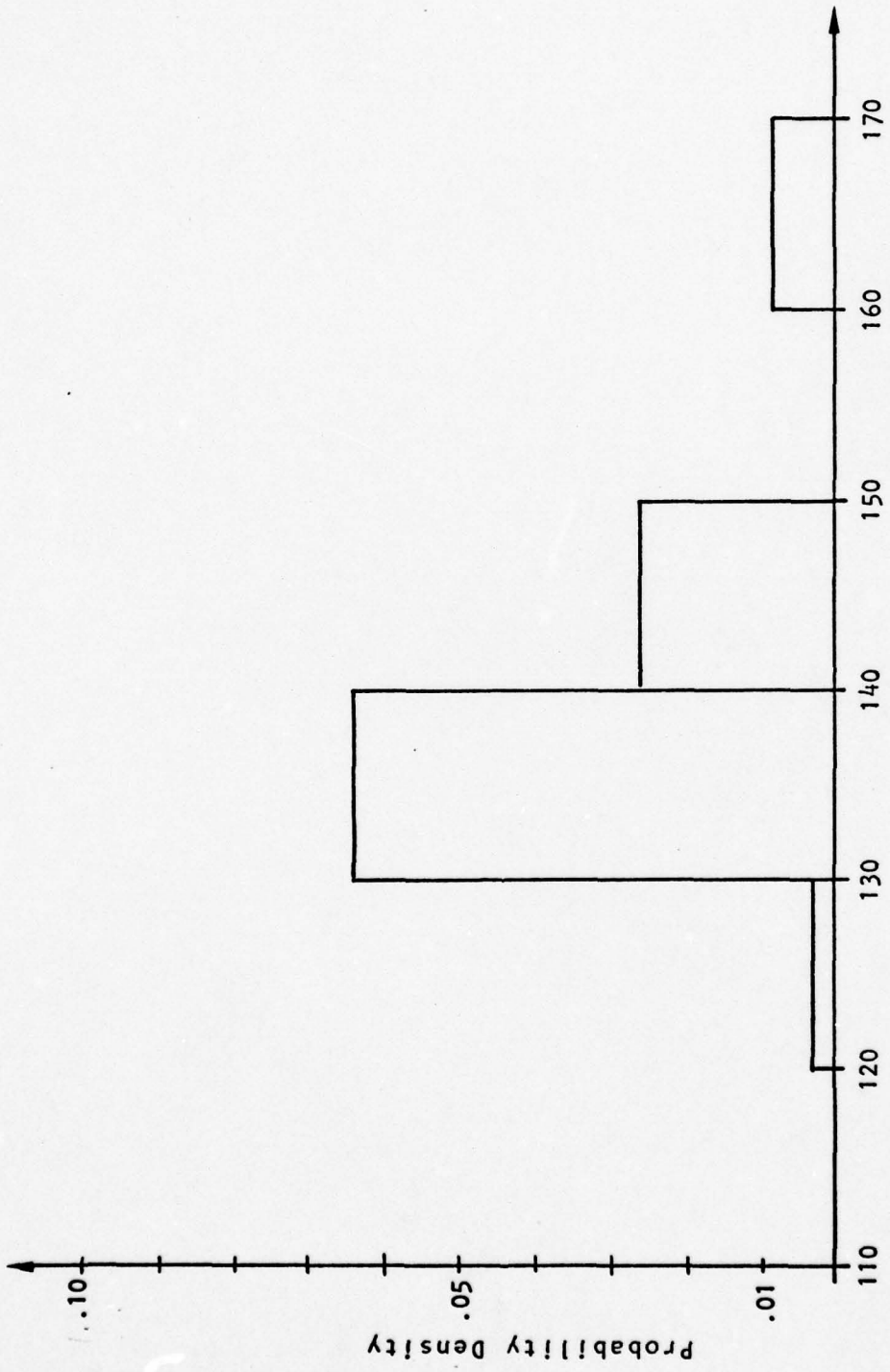

FIGURE 25 Broadband Source Level Distribution for Large Merchant Ships at 50 Hz.

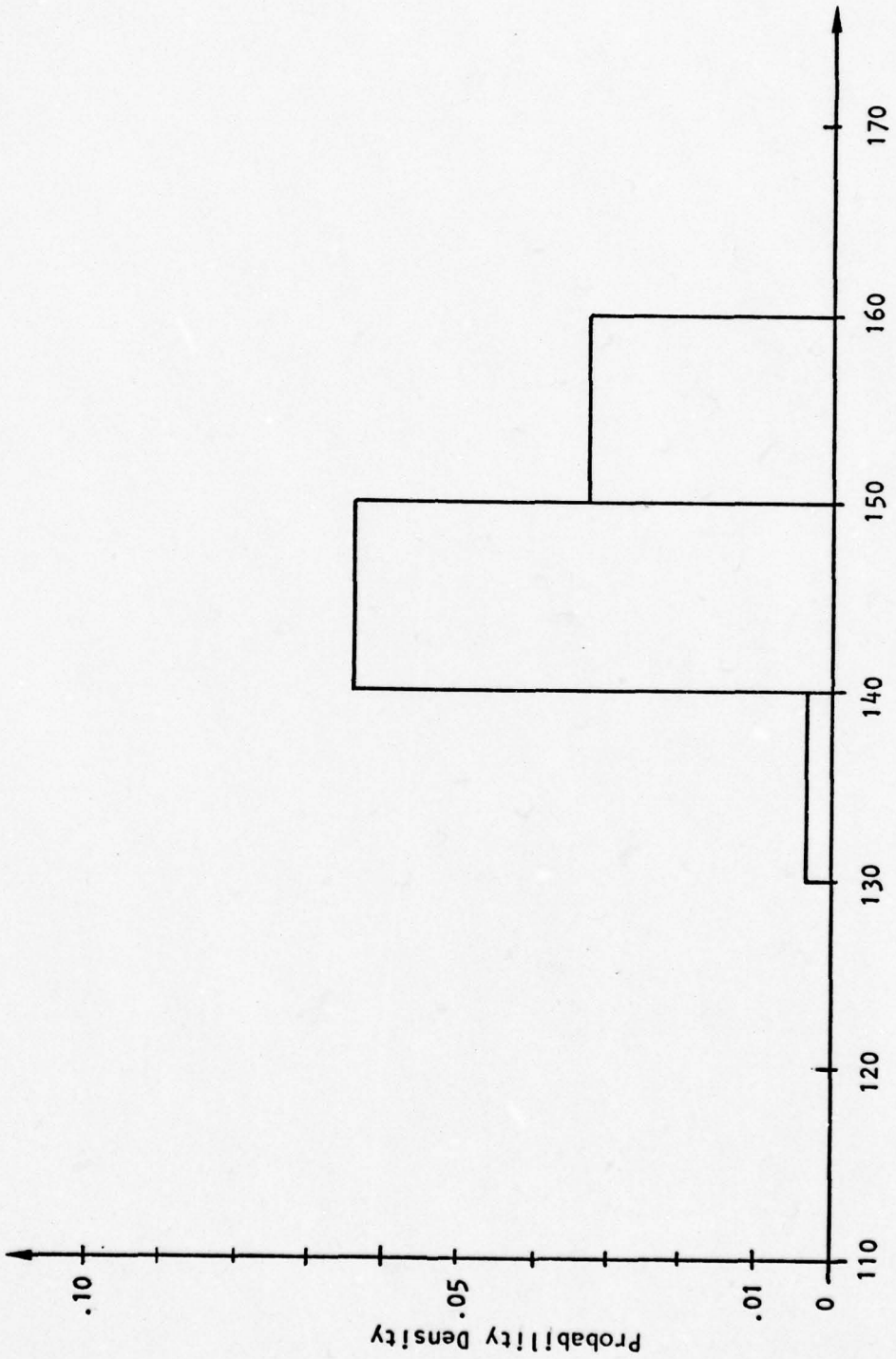

FIGURE 26 Broadband Source Level Distribution for Large Merchant Ships at 300 Hz.

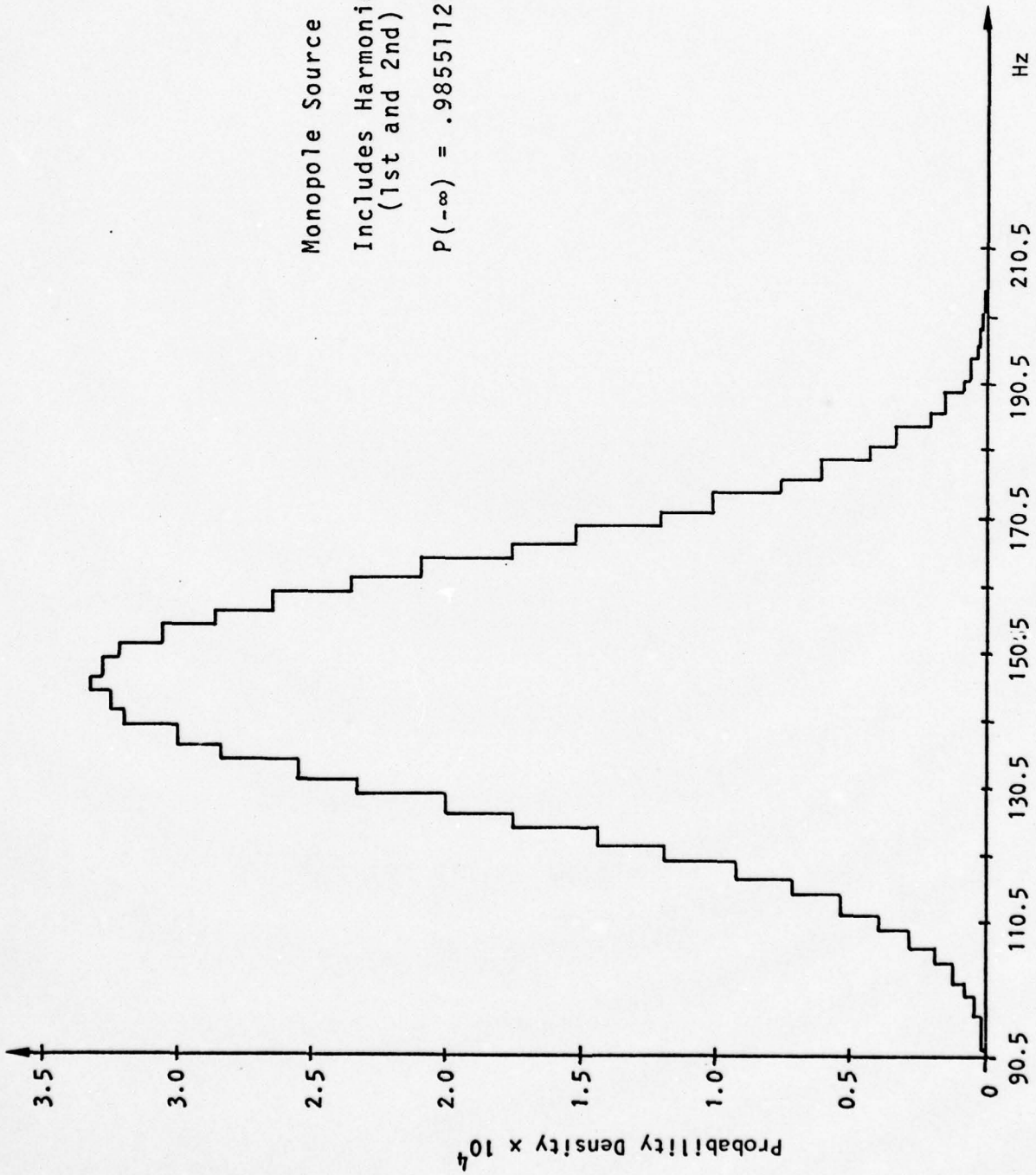

FIGURE 27 Blade Rate Source Level Density; Fishing Vessel, 40 Hz.

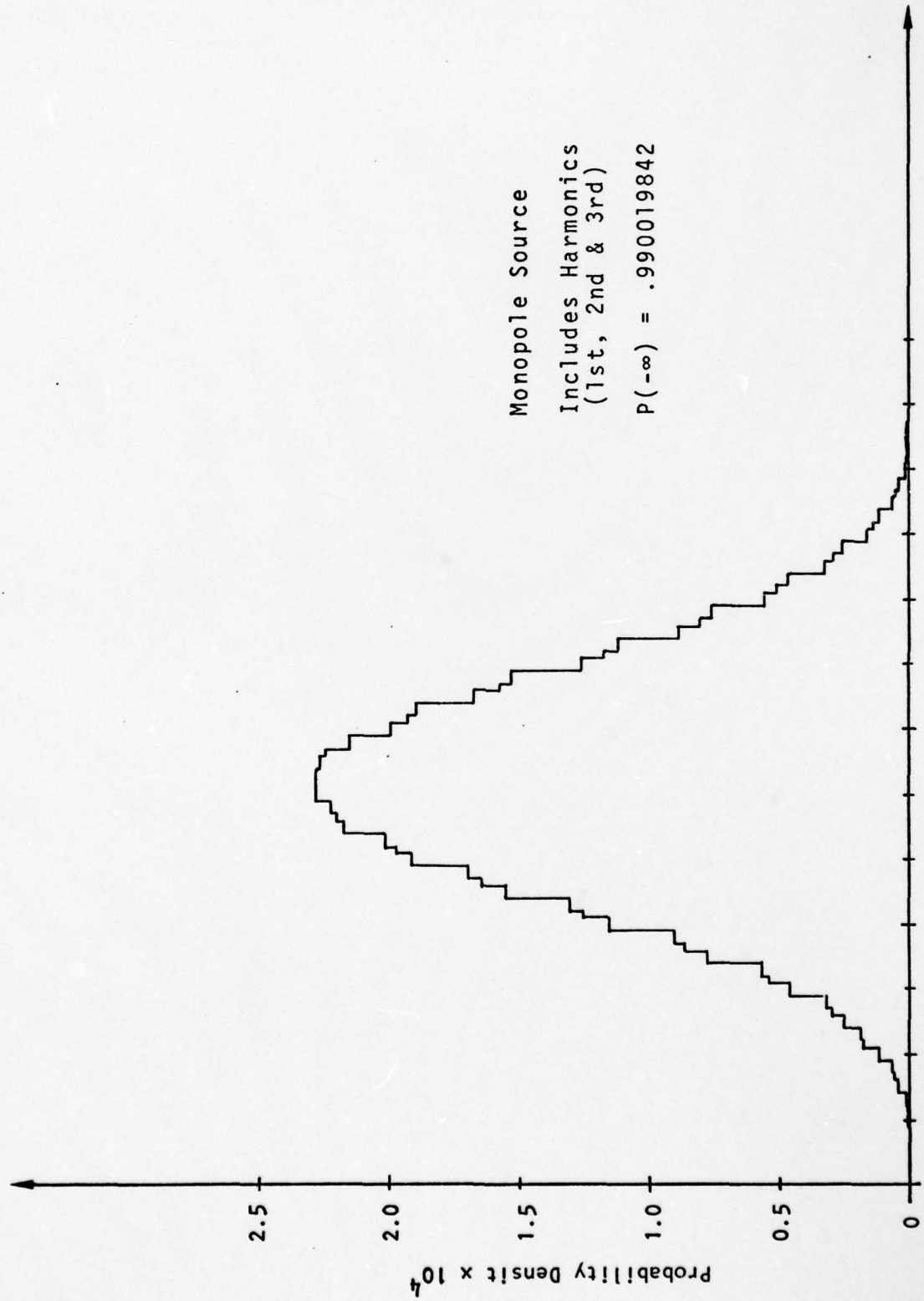

FIGURE 28 Blade Rate Source Level Density; Fishing Vessel, 50 Hz.

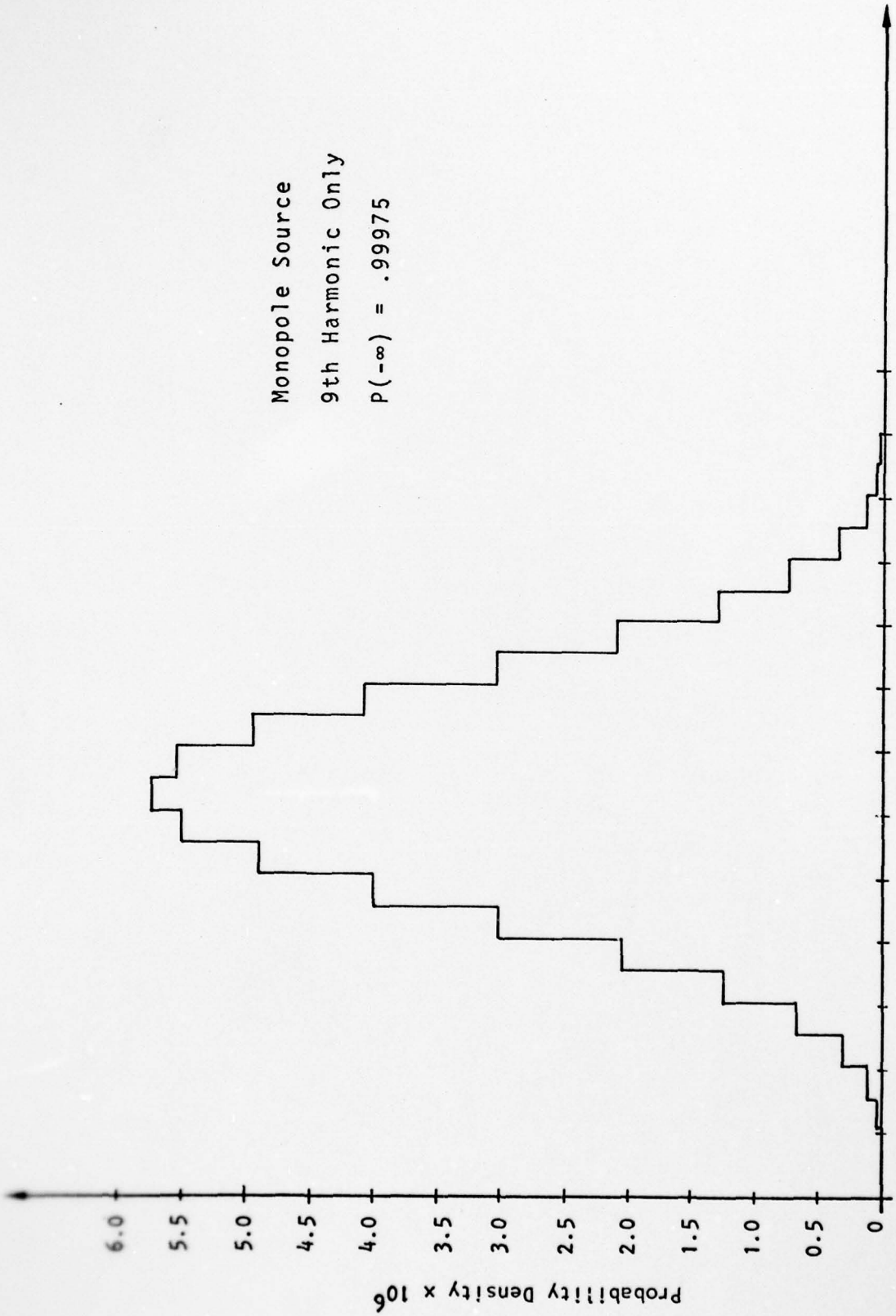

FIGURE 29 Blade Rate Source Level Density; Fishing Vessel, 300 Hz.

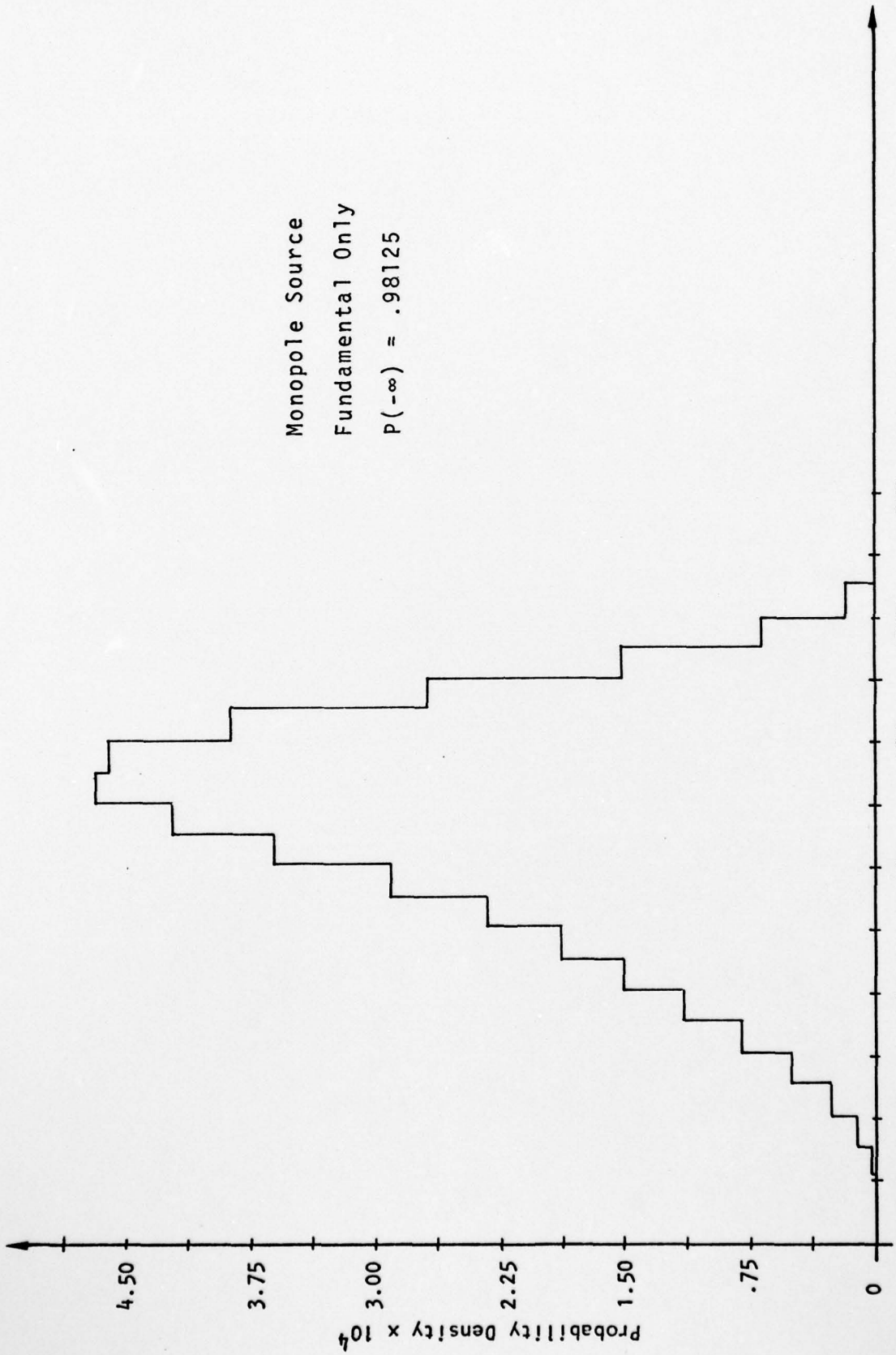

FIGURE 30 Blade Rate Source Level Density; Small Merchant Ship, 10 Hz.

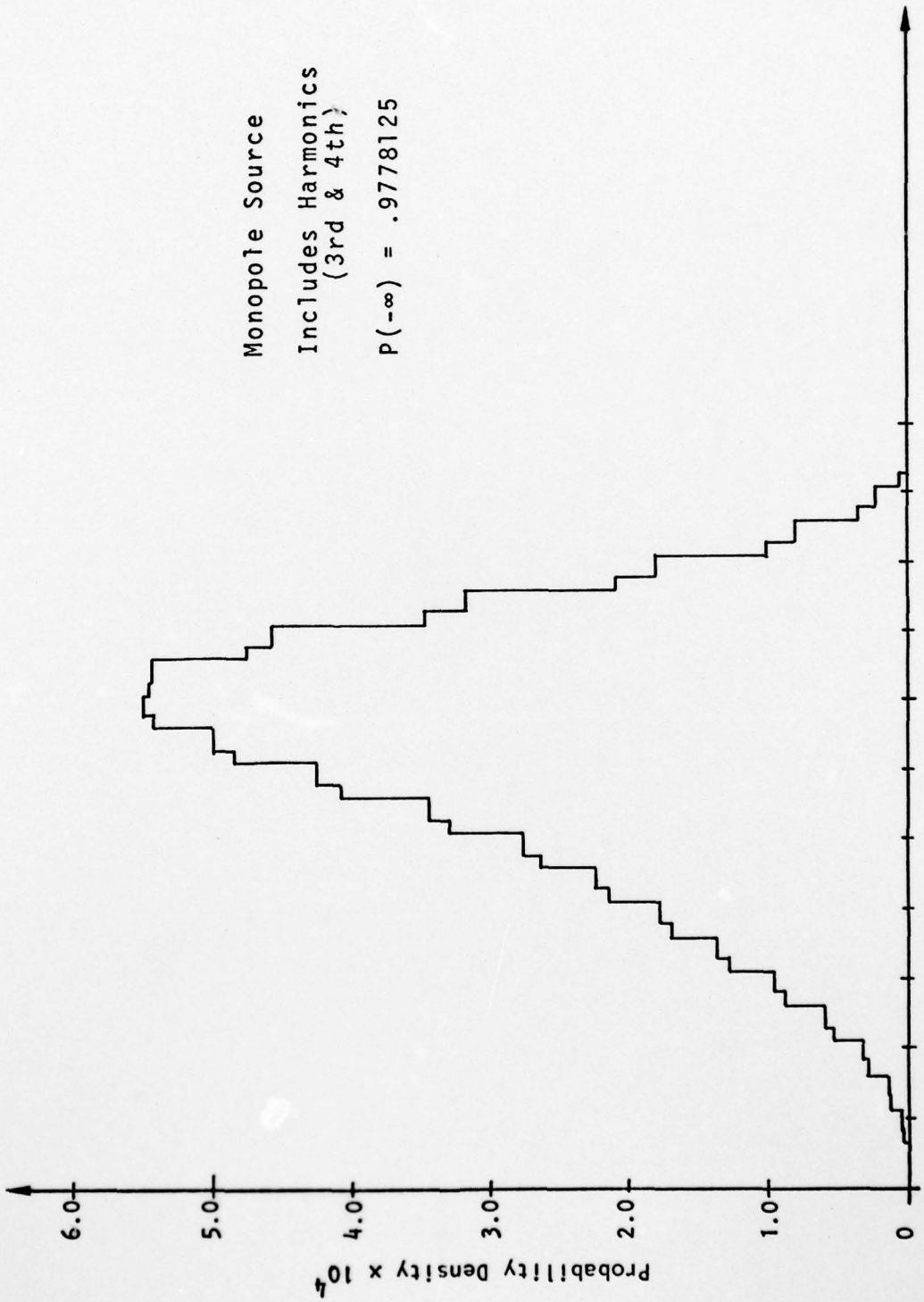

FIGURE 31 Blade Rate Source Level Density; Small Merchant Ship, 40 Hz.

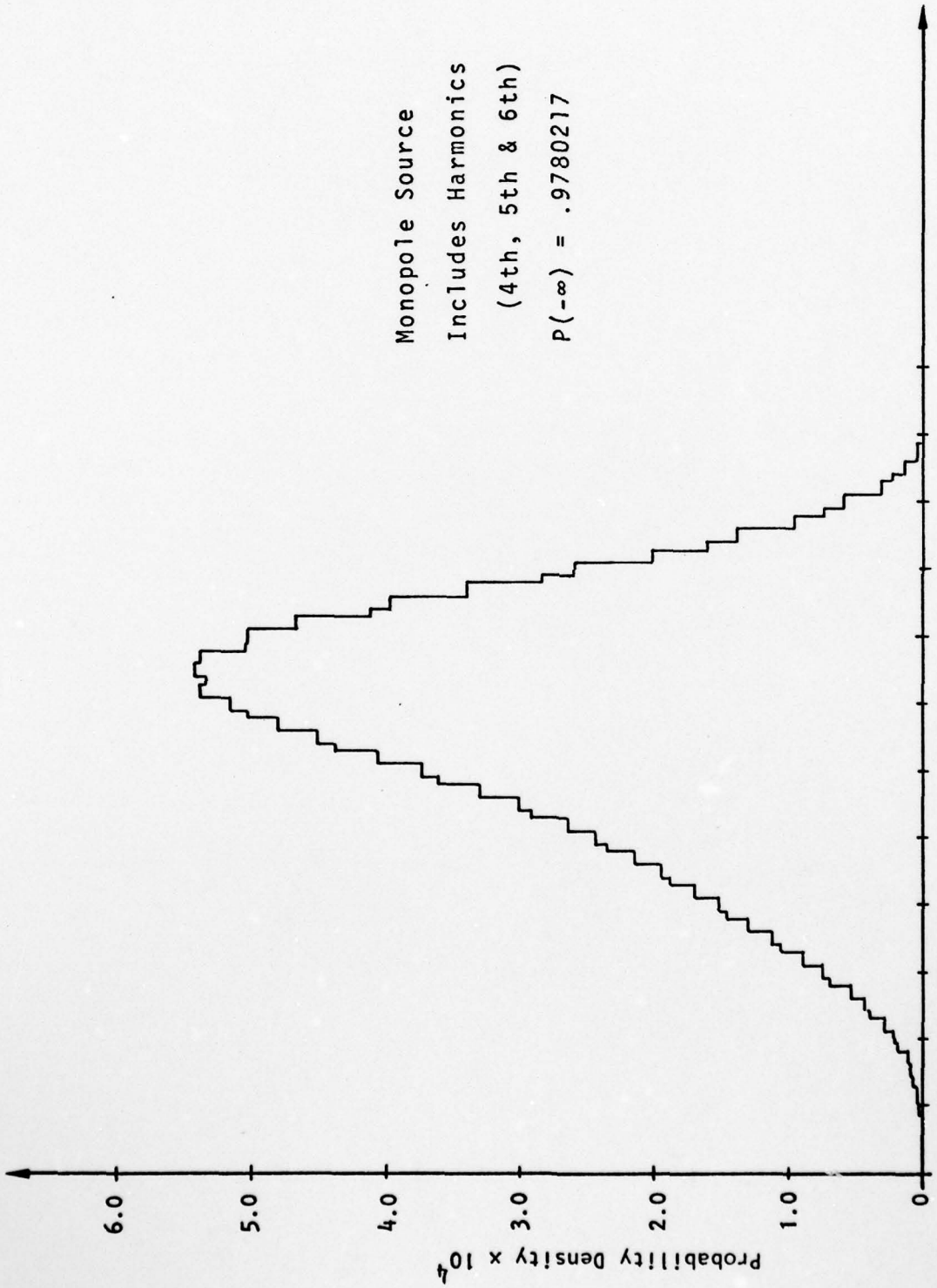

FIGURE 32 Blade Rate Source Level Density; Small Merchant Ship, 50 Hz.

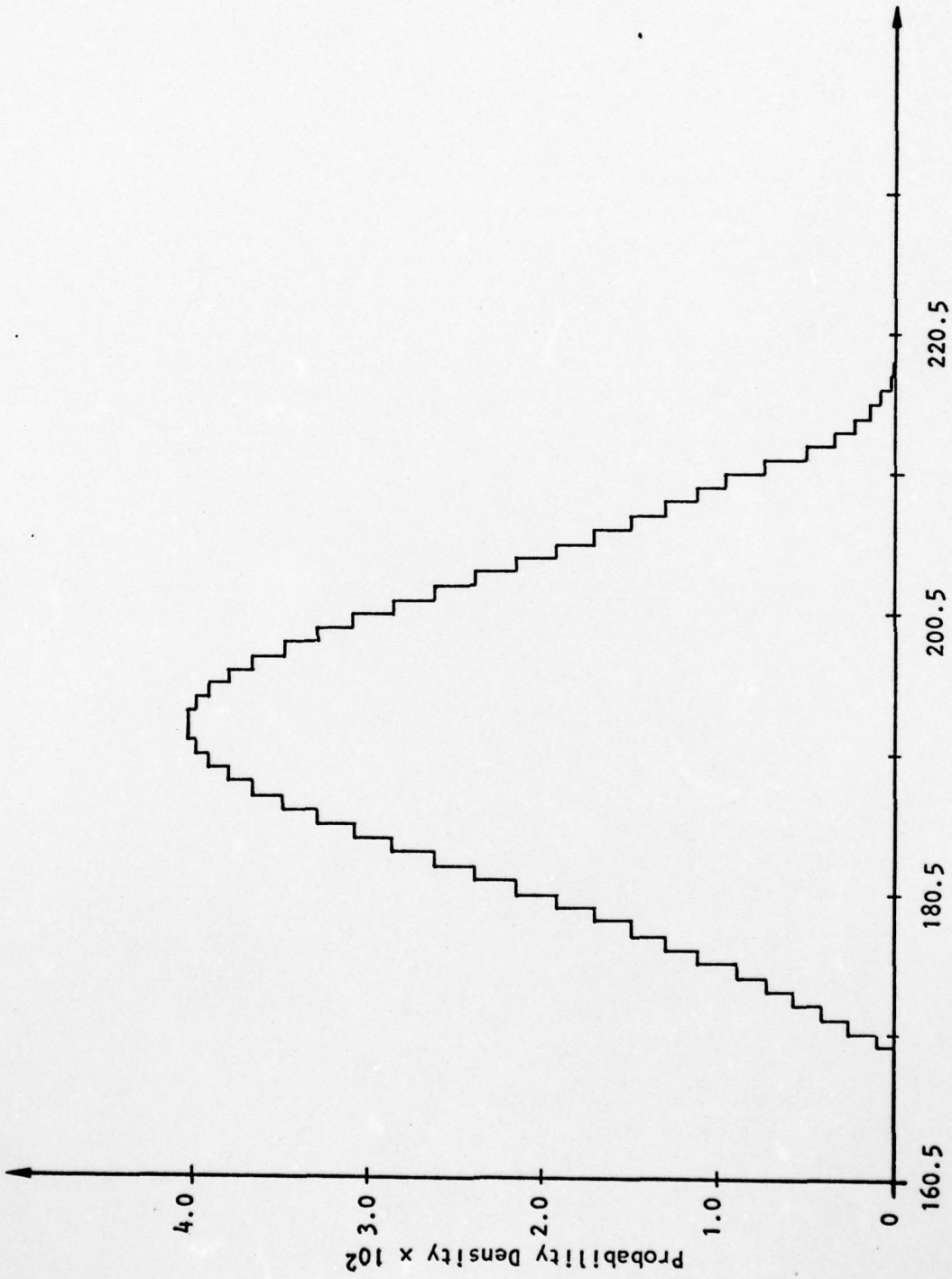

FIGURE 33 Blade Rate Source Level Density; Large Merchant Ship, 10 Hz.

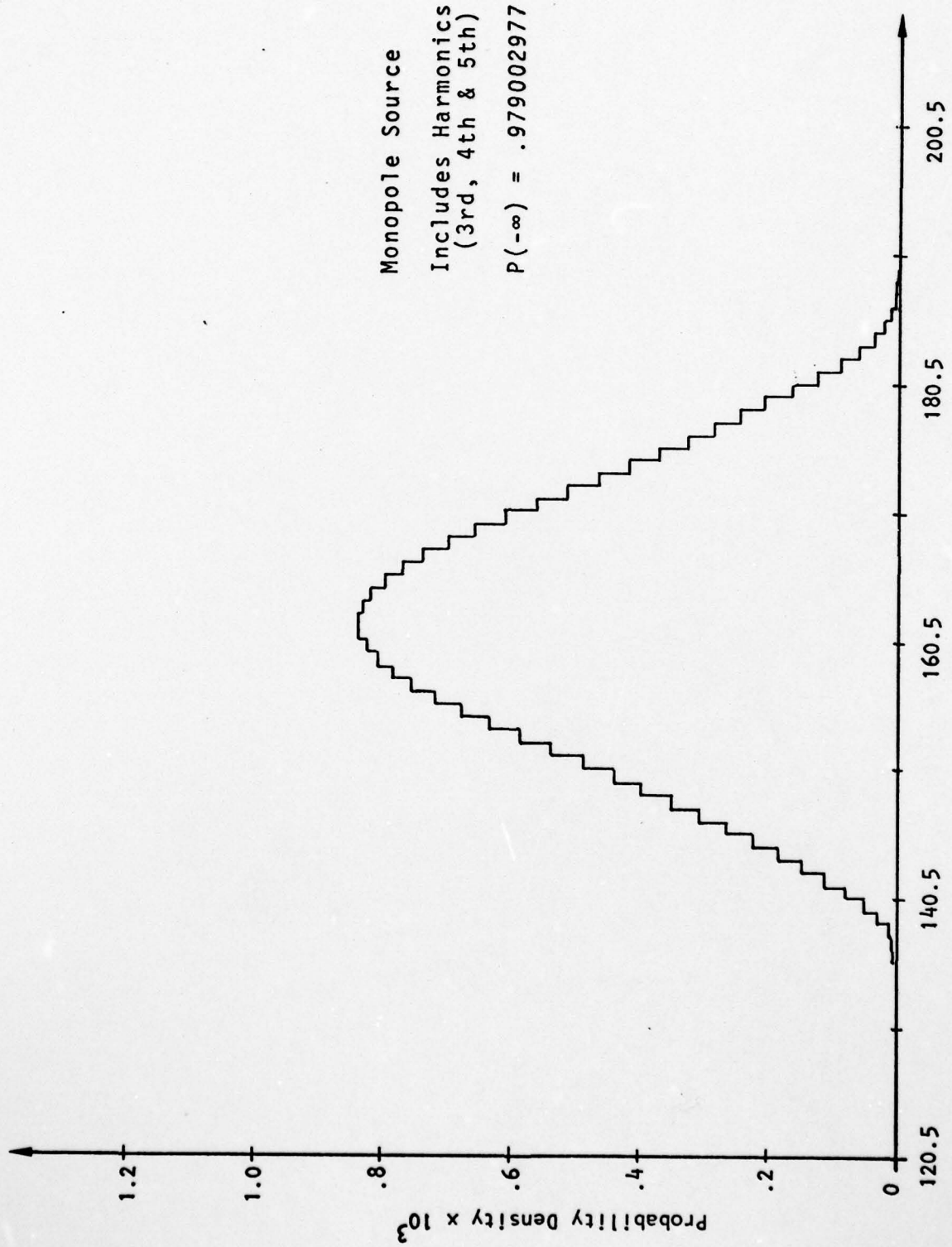

FIGURE 34 Blade Rate Source Level Density; Large Merchant Ships; 40 Hz.

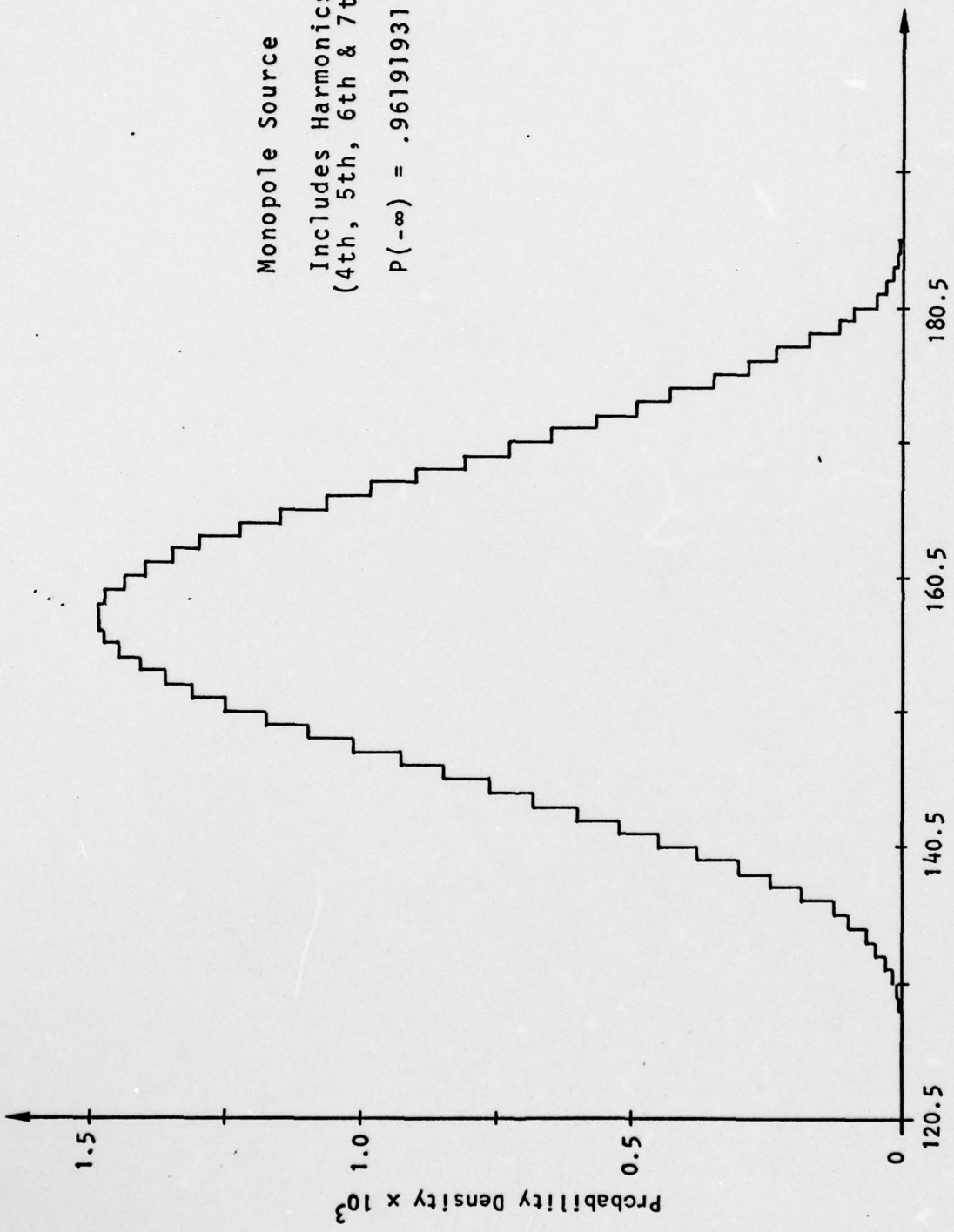

FIGURE 35 Blade Rate Source Level Density; Large Merchant Ship, 50 Hz.

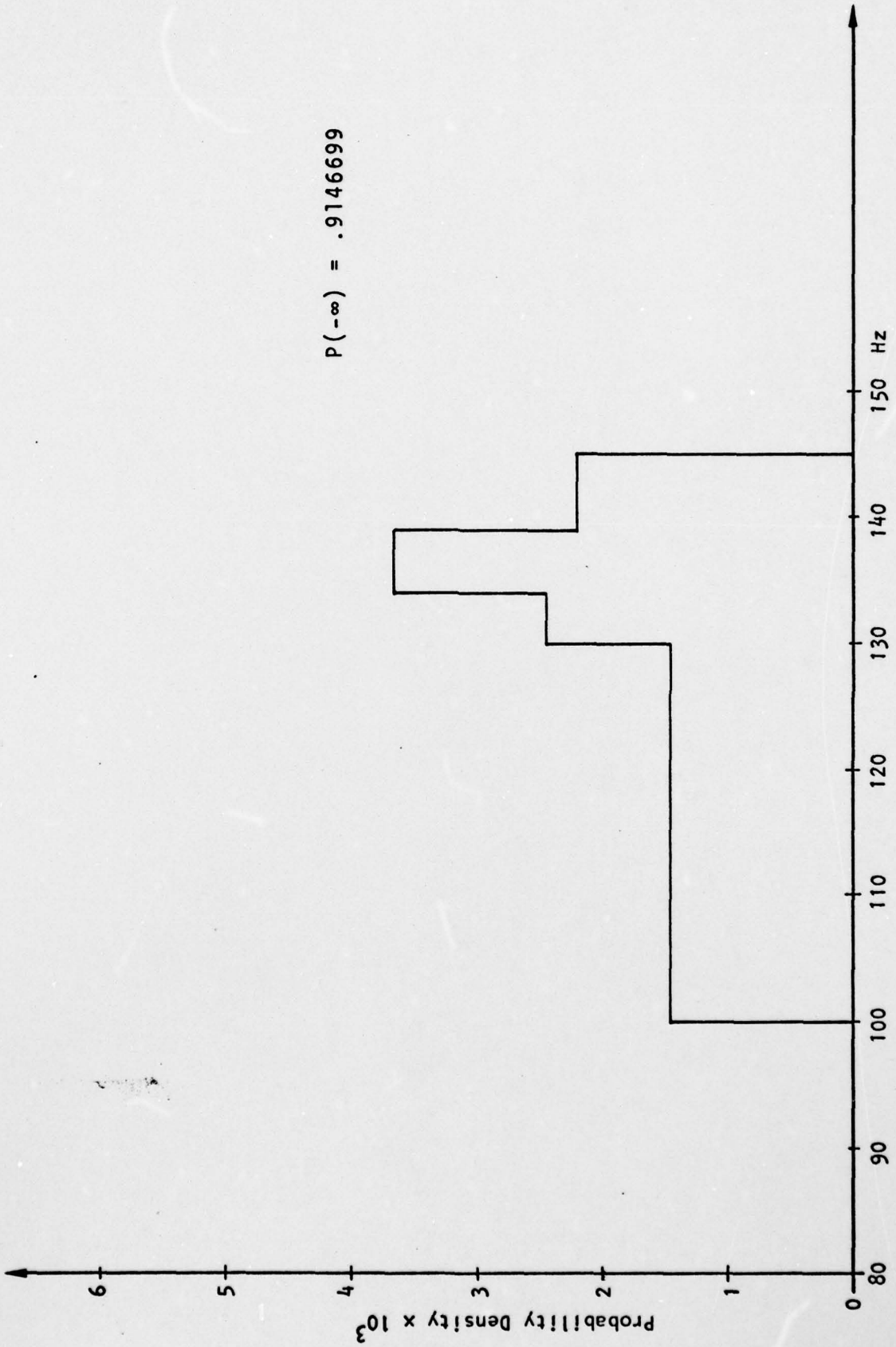

FIGURE 36 Narrowband Electric Plant Source Level Density; Fishing Vessel, 50 Hz.

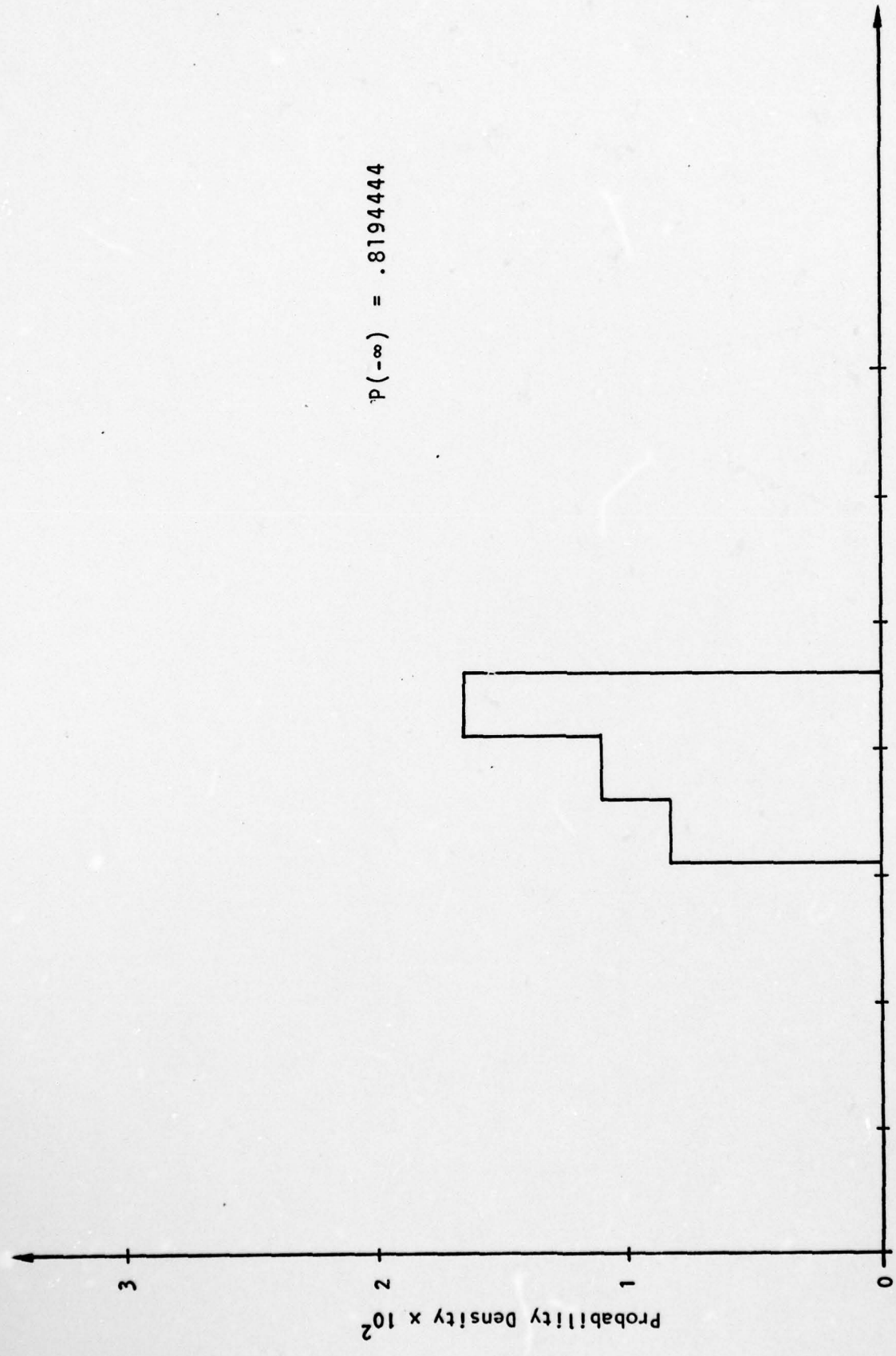

FIGURE 37 Narrowband Electric Plant Source Level Density; Small Merchant Ship, 50 Hz.

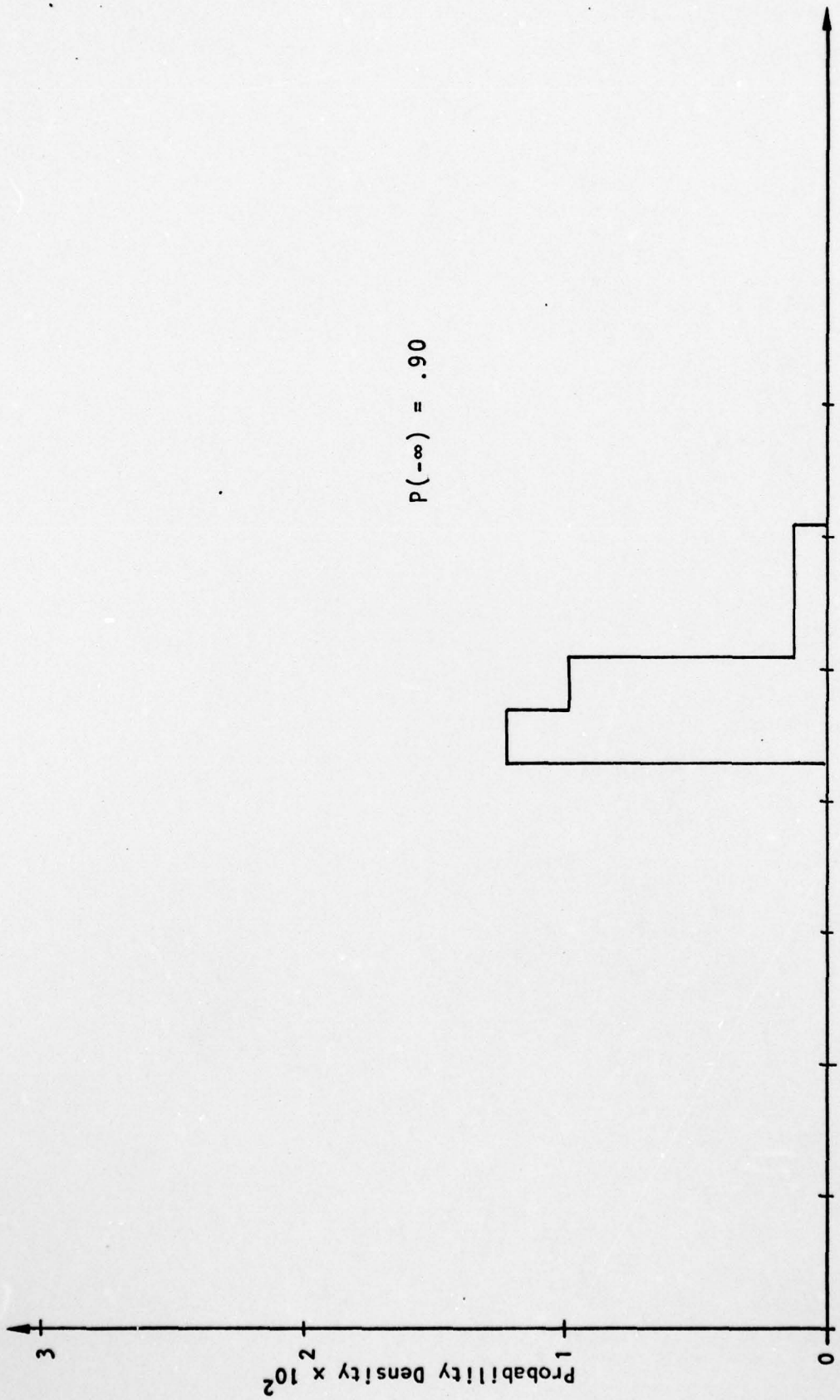

FIGURE 38 Narrowband Electric Plant Source Level Density; Large Merchant Ship, 50 Hz.

Revised information concerning the diesel firing rate and its harmonics are not yet available.

4.3.4 Means and Variances

The parameters required to establish the source characteristic functions are given in Tables 4 through 6, which gives means and variances for rms pressure in a 0.2 Hz band for monopole sources.

Table 4: Mean and Variance for Broadband Source

	Large Merchant	Small Merchant	Fishing	Frequency (Hz)
$m\ (\mu P)^2$	1.8106×10^{15}	6.6383×10^{14}	4.4093×10^{13}	10
$\sigma^2\ (\mu P)^4$	5.6936×10^{31}	9.3840×10^{30}	6.7276×10^{27}	10
m	1.1320×10^{16}	4.1505×10^{15}	2.5329×10^{14}	40
σ^2	9.1073×10^{32}	3.6672×10^{32}	2.6288×10^{29}	40
m	7.2416×10^{15}	2.6552×10^{15}	1.6204×10^{14}	50
σ^2	9.1073×10^{32}	1.5010×10^{32}	1.0759×10^{29}	50
m	8.8897×10^{9}	5.5417×10^{9}	3.4314×10^{9}	300
σ^2	2.4011×10^{28}	1.8089×10^{28}	8.4460×10^{27}	300

*Note: Monopole source rms pressure in a 0.2 Hz band.

Table 5: Mean and Variance for Blade Rate Source				
	Large Merchant	Small Merchant	Fishing	Frequency (Hz)
m $(\mu P)^2$	2.996×10^{18}	3.643×10^{17}	0.0	10
σ^2 $(\mu P)^4$	3.028×10	1.637×10^{38}	0.0	10
m	2.275×10	3.847×10^{14}	2.800×10^{15}	40
σ^2	2.223×10	1.612×10^{32}	1.528×10^{35}	40
m	1.633×10	1.035×10^{14}	7.850×10^{14}	50
σ^2	7.061×10	1.456×10^{31}	1.872×10^{34}	50
m	0.0	0.0	9.800×10^{9}	300
σ^2	0.0	0.0	9.783×10^{25}	300

*Note: Monopole source rms pressure in a 0.2 Hz band.

Table 6: Mean and Variance, Electric Plant Line at 60 Hz			
	Large Merchant	Small Merchant	Fishing
Mean $(\mu P)^2$	1.3671×10^{15}	3.1419×10^{14}	4.2394×10^{13}
Variance $(\mu P)^4$	7.0008×10^{31}	7.8622×10^{29}	7.7548×10^{28}

5.0 PREDICTION OF NARROWBAND COMPONENTS

The noise resulting from the operation of surface ships is not unlike that resulting from the operation of threat submarines. In particular, the presence of narrowband components (lines) in the radiated noise signatures of surface ships makes the acoustic detection of threat submarines more difficult. Predicting the effects of lines on the performance of surveillance systems requires either statistics or statistical measures. One measure of interference is the number of lines (1) whose center frequencies fall within a specified frequency interval Δf, and (2) whose intensities at the point of observation are greater than a specified threshold value t. If the threshold value t is appropriately selected, the measure is observable by means of narrowband analysis equipment.

The analysis which follows pertains to interference generated by ships in a specified sector of azimuth. Extension to array beam interference is discussed later.

The total number of lines satisfying the enumerated criteria is a random variable that can be expressed as the sum of contributions from individual ships:

$$N = \sum_{i=1}^{m} \sum_{j=1}^{n} \sum_{k=1}^{A_{ij}} N_{ijk} \qquad (102)$$

where m is the number of route envelopes intersecting the sector

n is the number of ship types

A_{ij} is the number of ships of type j on route i, a random variable

N_{ijk} is the number of lines satisfying the criteria radiated by ship k of type j on route i.

Each ship has several mechanisms that radiate narrowband fundamentals and harmonics; their effect is tallied by

$$N_{ijk} = \sum_{\ell=1}^{p} \sum_{h=0}^{\infty} U_{ijk\ell h} \qquad (103)$$

where p is the number of types of sources

$U_{ijk\ell h}$ is a random variable pertaining to harmonic h of source ℓ on ship k of type j on route i; its value is one if the enumerated criteria are satisfied, and zero if not.

The random variable $U_{iijk\ell h}$ can be expressed as a function of the characteristics or the source and of the medium:

$$U_{ijk\ell h} = e(F_{ijk\ell h})\ u\ [P_{ijk\ell h}\ z\ (G_{ijk}, Q_{ijk}) - t] \qquad (104)$$

where $F_{ijk\ell h}$ is the center frequency of the line designated by the subscripts

$P_{ijk\ell h}$ is the source intensity of the line designated by the subscripts

AD-A076 615 BOLT BERANEK AND NEWMAN INC ARLINGTON VA F/G 17/1
AN ALGORITHM FOR BEAM NOISE PREDICTION,(U)
MAY 79 M MOLL , R M ZESKIND , W L SCOTT N00173-77-C-0296
UNCLASSIFIED BBN-3653 NL

2 OF 2
AD A
076615

END
4-81

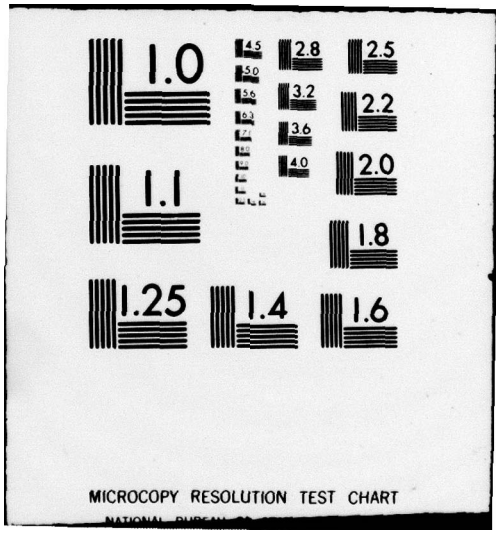
1.0
1.1
1.25
1.4
1.6
1.8
2.0
2.2
2.5
2.8
3.2
3.6
4.0
4.5
5.0
5.6
6.3
7.1
MICROCOPY RESOLUTION TEST CHART

G_{ijk} is the longitudinal (along the route) coordinate of the position of ship k of type j on route i; it is a random variable that is statistically independent of the longitudinal coordinate of any other ship.

Q_{ijk} is the transverse coordinate of the position of ship k of type j on route i; it is a random variable that is statistically independent of all other position coordinates.

$e(f) = 1$, if f is in Δf

$= 0$, if not

This function counts all of the lines in the designated frequency interval.

$u(x) = 1$, $x > 0$

$= 0$, if not

This function counts all lines whose intensities are above the designated threshold at the observation point.

Various statistical measures of the line count can be derived using (102), (103) and (104). For this initial effort, the ensemble mean or expected value will be derived. This measure is one that has been estimated in experimental work. The mean value of the line count is

$$m_N = E(N) \tag{105}$$

Substituting (102)in (105) and performing the expectation yields

$$m_N = \sum_{i=1}^{m} \sum_{j=1}^{n} \sum_{a=0}^{\infty} p_{ij}(a) \sum_{k=1}^{a} E(N_{ijk}) \qquad (106)$$

where $p_{ij}(\ )$ is the frequency function for A_{ij}. Since $E(N_{ijk})$ does not depend on the distribution parameter a [See (3)], all terms of the inner sum are equal, and

$$m_N = \sum_{i=1}^{m} \sum_{j=1}^{n} E(N_{ijk}) \sum_{a=0}^{\infty} p_{ij}(a)a \qquad (107)$$

The inner sum of (107) is the ensemble average $\bar{A}_{ij}$ of A_{ij}; thus,

$$m_N = \sum_{i=1}^{m} \sum_{j=1}^{n} \bar{A}_{ij} E(N_{ijk}) \qquad (108)$$

The expected value of (103) yields

$$E(N_{ijk}) = \sum_{\ell=1}^{p} \sum_{h=0}^{\infty} E(U_{ijk\ell h}) \qquad (109)$$

and the expected value of (104) can be stated as

$$E(U_{ijk\ell h}) = \int_0^\infty df\, f_{F_{j\ell h}}(f)e(f) \int_0^\infty dp\, f_{P_{j\ell h}}(p) \int_{R_i} dg \int dq$$

$$x\, f_{G_i}(g) f_{Q_i}(q) u[pz(g,q) - t] \qquad (110)$$

where R_i denotes a region which includes the intersection of the observation sector and the envelope of route i.

It will be assumed that the distribution of the coordinates G_{ijk} is uniform; furthermore, a change from the route variables to the observation variables simplifies the description of R_i. With these changes, the result is

$$E(U_{ijk\ell h}) = g_i^{-1} \int_{\Delta f} df\, f_{F_{j\ell h}}(f) \int_0^\infty dp f_{P_{j\ell h}}(p) \int_{R_i} dD \int dr|J(r,d)|$$

$$x\, f_{Q_i}(q) u[pz(r,D) - t] \qquad (111)$$

where g_i^{-1} is the arc length of the route in R_i.

Substituting (111) into (109) and the result into (108) gives

$$m_N = \rho \sum_{i=1}^{m} \sum_{j=1}^{n} k_{ij} \sum_{\ell=0}^{p} \sum_{h=0}^{\infty} \int_{\Delta f} df\, f_{F_{j\ell h}}(f) \int_0^\infty dp f_{P_{j\ell h}}(p)$$

$$x \int_{R_i} dD \int dr|J(r,D)| f_{Q_i}(q) u[pz(r,D) - t] \qquad (112)$$

where ρ is the earth's radius

$k_{ij} = \bar{A}_{ij} \div (\rho_{gi})$ is the average number of ships of type j on a unit length of route i.

Since z(r,D) is zero outside of the sector, it is clear that the integration on D can be restricted to the sector. The relationship between the route coordinates and the observation coordinates are given in Section 2.2 of Reference 1.

Reference 3 presents information on the narrowband source characteristics of three classes of ships: fishing, and small and large merchant. Histograms are given for the center frequency and source intensity generated by the propeller, the electric plant, and by the propulsion machinery. The histograms apply directly to the fundamental output, and can be modified to apply to harmonics. For the frequency histogram, the abscissa values are multiplied by (h + 1), where h is the harmonic number. Equations are given that relate the source level of a harmonic to that of the fundamental. The difference between the two is the amount by which the abscissa values are changed.

One could consider making Doppler corrections for the frequency histograms according to frequency, speed, and direction. For most applications, the correction will probably not be required.

Equation (112) pertains to the average number of lines received at a point that lie within a designated frequency band, that are above a specified threshold, and that are radiated by

ships in a designated azimuth sector. The result is readily modified for the prediction of array beam noise. For this case, the argument of the unit step function becomes

$$pz(r,D)b[D,E(r)] - t \qquad (113)$$

where $b(D,E)$ is the power gain function of the array-beamformer combination for a plain-wave arrival in terms of the azimuth and elevation angles.

The region of integration includes the entire azimuth sector between the points at which the route enters and leaves the acoustic basin. This accounts for the contributions of the sidelobes as well as the main lobe.

References

. M. Moll, R. M. Zeskind, and F. J. M. Sullivan, "Statistical Measures of Ambient Noise: Algorithms, Program, and Predictions," Bolt Beranek and Newman Inc. Report No. 3390, June, 1977.

. J. I. Mahler, F. J. M. Sullivan, and M. Moll, "Statistical Methodology for the Estimation of Noise due to Shipping in Small Sectors and Narrow Bands," Bolt Beranek and Newman Inc. Technical Memorandum No. W273, June, 1975.

. J. C. Heine and L. M. Gray, "Merchant Ship Radiated Noise Model," Bolt Beranek and Newman Inc. Report No. 3020, August, 1976.

. J. C. Heine and L. M. Gray, "A Statistical Model for the Acoustic Source Levels of Merchant Ships," Bolt Beranek and Newman Inc. Report No. 3814, July, 1978.

. L. P. Solomon, A. E. Barnes, and C. R. Lunsford, "Ocean Route Envelopes," Planning Systems, Inc. TR-036049, April, 1977.

. L. M. Gray, "Merchant Ship Blade Rate Probability Density Functions," Project Memorandum, March 9, 1978.

. L. M. Gray, "Estimates of the Source Levels for Blade Rate and Harmonics of Merchant Vessels," Project Memorandum, April 4, 1978.